Report IFJ PAN No 2104 / AP

The Plasma-Focus device at IFJ PAN Kraków:

Status and Perspectives

Marek Scholz, Agnieszka Kulińska

PODZIĘKOWANIA

Urządzenie Plasma Focus PF-24 w Laboratorium Źródeł Neutronowych (IFJ PAN) zostało zbudowane w ramach międzynarodowego projektu niewspółfinansowego Narodowego Centrum Nauki „Realizacja przez IFJ PAN zadań badawczych i inżynieryjnych związanych z budową stellaratora Wendelstein 7X, Faza 2" realizowanego w latach 2010-2013, decyzja nr 755/N-7XW/2010.

ACKNOWLEDGEMENTS

The Plasma Focus PF-24 device operating at the Laboratory of Neutron Sources (IFJ PAN) was constructed as part of the international grant of the Polish NCN National Science Center, contract No 755/N-7XW/2010 (2010-2013).

STRESZCZENIE

Raport prezentuje zasadę działania urządzenia Plasma Focus (PF) oraz opis zjawisk w prowadzących do generacji gorącej, gęstej namagnetyzowanej plazmy. Przedstawiono tutaj krótki zarys jego historii oraz aktualny stan badań, prowadzonych na tych układach w różnych laboratoriach na świecie. Na tym tle opisano specyfikację i parametry robocze PF-24, działającego w Laboratorium Źródeł Neutronowych (IFJ PAN) od 2014 roku. Przedstawiono aktualny stan zastosowanych systemów diagnostycznych oraz główne cele badań ilustrowane uzyskanymi wynikami. Przedstawiono plany i perspektywy przyszłych eksperymentów oraz związane z nimi tematy prac doktorskich.

ABSTRACT

The report presents the principle of operation of the Plasma Focus (PF) device and a description of the phenomena in the generation of hot, dense magnetized plasma. Here is a brief outline of its history and the current state of research conducted on these systems in various laboratories around the world. Against this background, the specification and operating parameters of PF-24, operating at the Laboratory of Neutron Sources (IFJ PAN) since 2014, have been described. The current state of the diagnostic systems used was presented as well as the main research objectives illustrated by the results obtained. Plans and perspectives for future experiments as well as related topics of doctoral dissertations were presented.

CONTENTS

PODZIĘKOWANIA 3

ACKNOWLEDGEMENTS 3

STRESZCZENIE 5

ABSTRACT 5

1. INTRODUCTION 9

1.1. History and background 9

1.2. Comparison of the PF-24 system with systems working in other laboratories 12

2. BRIEF DESCRIPTION OF PHYSICAL PHENOMENA OCCURRING IN PLASMA-FOCUS DEVICE 13

3. 1. Design of the PF-24 device 20

3. 2. Diagnostics equipment 25

3. 3. Measurements of the Current Generator's Parameters of the PF-24 Device 27

4. THE MAIN AIMS of STUDIES, RESULTS and PERSPECTIVES 29

4. 1. Neutron emission measurements 29

4.2. Radiative collapse 31

4.3. BCF-12 detectors test 32

4.4. Proton – boron nuclear reaction in Plasma-Focus device 35

5. PROPOSED OF PHD THESIS 41

5.1 The phenomenon of radiation compression in the gas mixtures for the PF-24 device 41

5.2 The study of the proton boron (pB) reaction rate in the Plasma-Focus device. 42

6. SUMMARY 42

REFERENCES: 45

1. INTRODUCTION

1.1. HISTORY AND BACKGROUND

Plasma-Focus (PF) device belongs to Z-pinch family and it is modification of a gaseous, linear Z-pinch. The name of Z-pinch specifies a cylinder of plasma in which current is driven in the *z* direction by an electrical power source, usually condenser bank. In this configuration of the plasma with the current an azimuthally directed magnetic field (B_θ) tends to compress and confine the plasma (Fig. 1).

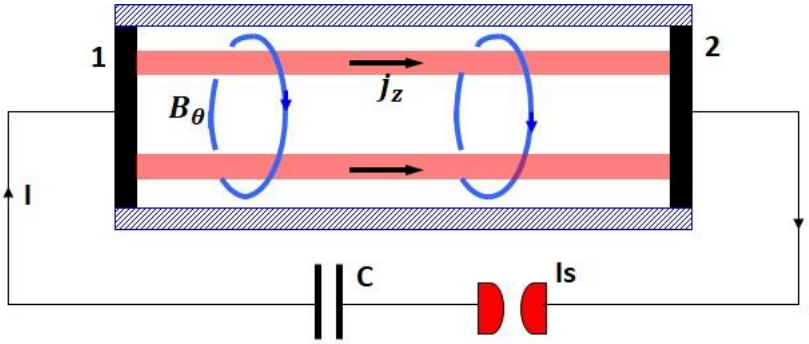

Fig. 1. Linear Z-pinch geometry. The electric charge accumulated in the condenser C, by the spark gap Is, produces in the circuit current I and current j_z in gas inside the cylinder between electrodes 1 and 2 as a result of the current flow, a magnetic field B_θ is created that compresses the plasma.

The modification of the device electrodes from the gaseous, linear Z-pinch to the PF configuration, was done in such a way as to move the high-temperature plasma away from the insulator separating the electrodes, but while maintaining the idea of a classic Z-pinch system. [SCHOLZ, 2016]. In the 1950s and the early 1960s, two configurations of the PF system were developed. First was developed in Kurchatov Institute by Filippov [FILIPPOV ET AL., 1962] as a modification linear Z-pinch with metallic walls and second developed in Los Alamos by Mather [MATHER, 1965] as a modification of plasma coaxial accelerator which operated at a high gas pressure. The main difference between these two systems lies in the geometry of electrodes; namely, the ratio of the anode diameter to its length, (a/l). In a Filippov-type system $a/l > 1$, while the ratio for Mather geometry is $a/l < 1$ (see Fig. 2). Despite the differences in design, the final characteristics of plasma proved to be very similar as a result of physical processes occurring in these systems.

From that moment these devices to be called Filippov's or Mather's type Plasma-Focus systems.

At the beginning, experiments carried out on PF devices were oriented towards fusion research. Strong deuterium ion compression can lead to nuclear reaction d + d = n + α (in short: dd) and the resulting neutron flux can be experimentally observed. The first experiments (1954 ÷ 1957) carried out using a PF system showed a significant increase dd reaction rates as compared to the linear Z-pinch. Using a camera with collimators the location of the neutron source was determined. The neutron source was formed on the axis, near the

anode of a PF system. Furthermore, measurements using magnetic probes showed that the gas discharge starts along the insulator, and plasma is created by compressing gas to the anode axis then extends along the axis of the system and is not strictly cylindrical as in the conventional linear Z-pinch.

Fig. 2. Schematic view of Mather (a) and Filippov (b) type Plasma-Focus (PF) systems; 1 – anode,

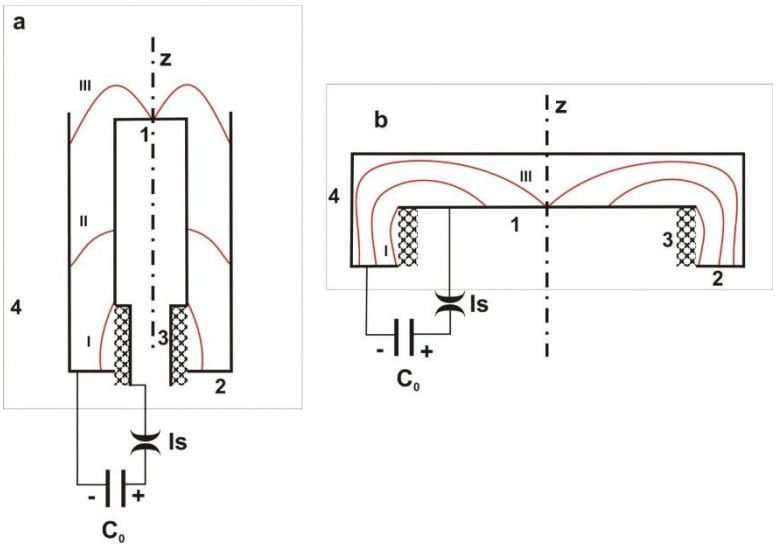

2 – cathode, 3 – insulator, Is – spark gap, C_0 – power supply (capacitor bank). I – discharge phase, II – acceleration phase (Mather-type system only), III – radial movement of the layer and creation of the plasma focus [SCHOLZ, 2016].

In the early 1960s, physicists used PF devices obtaining deuterium plasma of high density, with relatively high plasma temperature and high neutron reaction rate. Moreover, they found that physical processes leading to the formation of plasma in the Plasma-Focus are very similar regardless of the size of the energy source. Next, the experiments showed that, the total output of neutrons, i.e. the rate of fusion reaction, linearly depends on the fourth power of current flowing in the plasma, or in the second power of energy stored in the power source of PF systems (Fig. 3).

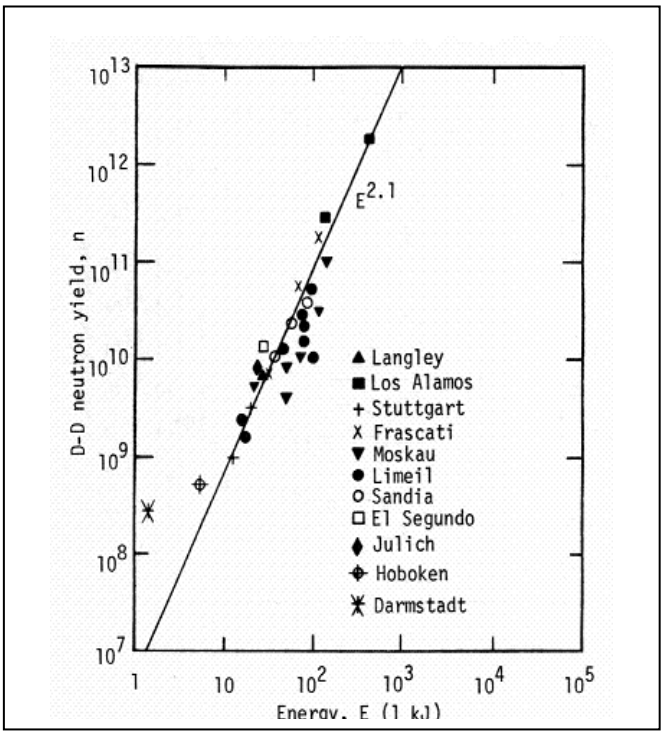

Fig. 3. Scaling law for the total emission of neutrons as a function of energy supply from capacitor banks collected in 1974 [MICHEL, 1974].

Experimental data obtained at that time allowed the assumption, that the PF systems on a larger scale, in according to this scaling law, can be achieved 'breakeven' (i.e. the power being released by the fusion reactions is equal to the thermal energy of plasma).

At the end of the 1970s, Plasma -Focus devices with energy source around 1 MJ and higher started to operate. At so, at the Kurchatov Institute a Filippov-type device with nominal capacitor bank energy of 3 MJ was built. In turn, at the ENEA Institute in Frascati, a system with nominal capacitor bank energy of 1 MJ was designed. This system could operate with two electrode types: Mather and Filippov. Another system that was working at the University of Stuttgart at that time was the Plasma-Focus device with an energy source of about 0.7 MJ.

The results obtained during research using PF systems in Frascati and Stuttgart have shown that increasing the energy level in the capacitor bank, above about 0.5 MJ, does not increase the overall rate of nuclear fusion. It was explained in such a way that only part of the total current of the PF system flows in the pinch [MICHEL, 1974]

This was thought to have been the main reason for the inhibition of the increase in total neutron emission from large PF systems. In addition, it turned out from the measurement of neutron emissions that the plasma in the pinch is not in thermal equilibrium and its ion temperature is not high. It caused the discontinuation of further development of large PF systems because it was considered not possible to build a self-heating fusion reactor with such a configuration.

The similar research was performed on the PF Poseidon system at the University of Stuttgart and one observed the same effect of the lack of the increase in total emission of neutrons with increasing energy stored in the capacitor bank. However, changing the conditions of the current flow in the vicinity of the insulator by changing the material of the insulator separating the electrodes of the system showed that it was possible to overcome this effect of saturation of the total neutron emission from pinch plasma [HEROLD ET AL., 1989]. The last of the large Plasma-Focus systems, PF-1000, with a capacitor bank energy equal to 1 MJ, was launched at the Institute of Plasma Physics and Laser Microfusion, in Warsaw in the 1990s.

Throughout 50 years of research on plasma produced in PF systems many experimental and theoretical results were published, and the some important results were summarized in following reviews: [BERNARD ET AL., 1988; GRIBKOV AND FILIPPOV, 1979; FILIPPOV, 1983; DECKER AND WIENECKE, 1976; SCHOLZ, ET AL., 2004; SADOWSKI AND SCHOLZ, 2008].

However, these results have shown that Plasma-Focus systems have not completely exhausted their potential in research related to controlled thermonuclear fusion. Admittedly, the prospect of these systems as a fusion reactor seems very limited in the light of experimental facts, but they enable relatively easy obtainment of the parameters of plasma in which the reaction rate of fusion is very high. This provides an opportunity to study the conditions in which these fusion reactions occur and the properties of emission of the products of these reactions in plasma which is not in a thermodynamic equilibrium.

1.2. COMPARISON OF THE PF-24 SYSTEM WITH SYSTEMS WORKING IN OTHER LABORATORIES

Currently, many laboratories around the world are conducting experiments using Plasma-Focus systems. Most of them use small PF systems with source energy at the level of single kJ for research. They are installed at universities to train doctoral students in plasma physics and diagnostics. In some laboratories, they are used for the interaction of streams and plasma with materials such as tungsten or molybdenum. An interesting scientific program on such systems is implemented in Chile, where devices with a power supply below 1 kJ are used to study the interaction of X and neutron radiation with genetic material [SOTO ET AL., 2008].

In the case of PF systems with maximum power sources above 0.5 MJ, the PF-3 systems in Kurchatov and PF-1000 in IPPLM still work but the scientific programme on these devices are mostly devoted to plasma physics or generation of plasma jets. Now, both of them operate with low energy below 0.5 MJ.

The newest PF systems are: TallBoy and GEMINI systems with 0.5 MJ and 1 MJ maximum power sources, respectively. Both of these systems were built and launched at National Security Technologies, Las Vegas, NV, United States in cooperation with the University of Nevada Las Vegas. Both were created to check the scaling law and as intensive sources of fast neutrons [BENNETT ET AL, 2017].

In this group, the PF-24 system with the maximum energy of a 100 kJ power source is currently the only system in the world from this energy range. Thanks to this, it is a very flexible system for experiments in various fields of plasma physics, as in the case of PF

systems with low power supply. On the other hand, it has such a high power supply that it allows studies related to the rate of fusion reaction under different conditions and for different isotope mixtures.

Considering the results of the research carried out on different PF systems, the research program can be targeted at explaining the phenomena associated with the evolution of plasma and its impact on the reaction yield of fusion in plasma for different kind of light nuclei.

The purpose of experiments carried out as a part of this program can be to verify results obtained thus far on large PF systems related to the escape of current flowing through plasma; and to show and the role of epithermal light ions (for example deuterons) in the interaction with plasma of a pinch. Understanding these processes will enable development, based on a Plasma-Focus device, of intense, pulsed sources of fast neutrons for research related to controlled thermonuclear fusion. It would also allow the testing of detectors dedicated to thermonuclear device diagnostic systems.

The PF-24 is the Mather-type device [MATHER, 1965]. The maximum energy stored in condensers at 40 kV is about 100 kJ. Compared to the discussed devices, Plasma-Focus in IFJ PAN is placed as a medium power device (100 kJ), which can be used for basic research of high-temperature plasma for various gases and their mixtures. In this report will show already completed research projects made using PF-24 as well as future research plans.

2. BRIEF DESCRIPTION OF PHYSICAL PHENOMENA OCCURRING IN PLASMA-FOCUS DEVICE

The conceptual design of a plasma focus device is shown in Fig. 4. The discharge chamber is pre-filled with a given working gas, e.g.: deuterium at a pressure of $p = 0.5 \div 15$ mbar, depending on the PF-mode of operation and/or type of electrodes. The specified pressure range depends on the geometry of the individual electrodes and the parameters of the power source circuit.

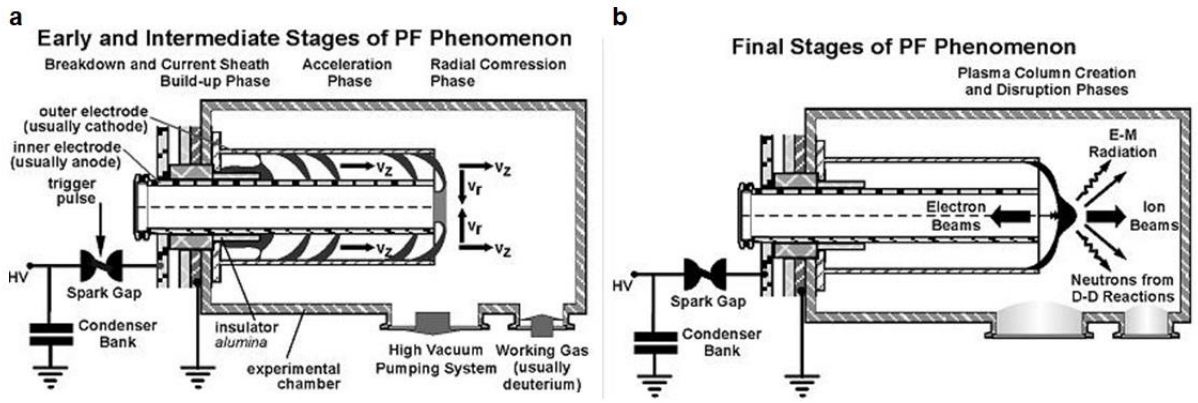

Fig. 4. Plasma focus phenomenon in the Mather type Plasma-Focus device. (a) An early and intermediate stages of PF phenomenon, (b) final stage of PF phenomenon.

The plasma-focus operation can be divided into the following phases:

Breakdown, Plasma Sheath (PS) formation and take-off

The basic processes leading to the formation of a conductive plasma sheath (PS) are characteristic of the electrical discharges in gases. But one can be taken into account, that in Plasma-Focus device the electrical discharge occurs within a cylindrical geometry of electrodes along the insulator, for pressures ranging from $1.3 \cdot 10^2 \div 1.0 \cdot 10^3$ Pa, and voltage at the capacitor bank of over 16 kV.

Thus, at the beginning of the discharge, the electrode geometry determines the electric field distribution in the gas between the electrodes. Initially, the value of this field is the largest on the cathode – insulator boundary, and even though gas ionization with an electric field takes place in the whole area between electrodes, then development of the ionization wave is the fastest along the insulator. In this way the formation of a thin layer of ionized medium with a low degree of ionization and cylindrical symmetry, short-circuiting the cathode and anode [SCHOLZ ET AL., 2005].

Resistance of this short-circuiting of the cathode and anode by thin layer of partially ionized plasma decreases with increasing concentration of electrons n_e, caused by gas ionization. [BRAGINSKI AND MIGDAL, 1958]. As the result of ionization and increase in n_e, there is a rapid drop in resistance $\tilde{R}$, which lasts from dozens to hundreds of nanoseconds depending on the scale of the device.

Ensuring azimuth symmetry of PS is very important due to the subsequent phases of the discharge development in the Plasma-Focus system; namely, gas sweeping during acceleration PS and symmetrical plasma compression in the last phase of the phenomena leading to the formation of a plasma focus.

In summary, it can be said that the formation of a symmetrical and uniform plasma sheath (PS) significantly affects the parameters of the plasma focus. Consequently, thin conductive plasma sheath (PS) is forming near the surface of the insulator.

As the number of ions increases during ionization, directed movement of working gas molecules in the PF chamber. At some point, the number of ions and electrons will become so large that the plasma sheath will be impermeable to the particles of the working gas. In this way, PS is capable of transferring the pressure of the magnetic field to the gas molecules filling the PF chamber. Summarize; one can say that a "magnetic piston" is created, capable of sweeping the gas.

Due to the fact that the current in the plasma sheath grows rapidly, then PS breaks away from the insulator and begins to move under the magnetic force $\vec{B} \times \vec{j}$, where $\vec{B}$ is the induction of magnetic field and $\vec{j}$ is the density of the current flowing in the PS. Then, as soon as the magnetic structure of the piston is formed, it will also sweep gas in the space between the electrodes of the PF system.

Run-down phase of the plasma sheath (PS)

This phase occurs in the Mather type electrodes only. After its formation, the PS as a magnetic piston begins a lift-off from the insulator surface due to the $\vec{B} \times \vec{j}$ magnetic force, and accelerates in the direction of the electrode muzzle.

The current in the PS grows very fast, so that velocity of the PS reaches a velocity greater than the speed of sound in the working gas in inter electrode space, at the beginning of its movement along the electrodes. This leads to the formation of a shock wave in the gas.

In this way, a structure called plasma sheath consists of the shockwave, plasma layer and magnetic piston. This structure is moving along the electrodes in the Mather system with the velocity ca. $(10^6 \div 10^7)$ cm/s, into an unperturbed working gas region. Thickness of the structure is typically < 1 mm and corresponding to the free mean path of neutrals. Its Mach number at this point is of the order of 100. Gas molecules pass through this front in about 1ns. This time is about two orders of magnitude smaller than the ionization relaxation time. Therefore, in this structure exists a not equilibrium, transition region, with a temperature of several eV. It gradually passes into a fully ionized plasma layer ($kT_e \sim (10 - 20)$ eV, $n_e \sim (10^{17} - 10^{18})$ cm^{-3}) in equilibrium. Thus summarizing, the plasma sheath can be ideally defined as a complex spatial structure between undisturbed inert gas and a "magnetic piston" consisting of a dense and hot neutral layer, ionization layer, and plasma layer, through which current flows, and behind which there is vacuum (or very low density plasma) with a magnetic field.

The dynamics of the run-down acceleration phase and the following compression phase are fairly well described by Newton's Second Law and by the circuit equation. Thus, sweeping of the working gas, the dynamic properties of the PS during acceleration along the electrodes, and compression can be described by a simple model of a two-dimensional snow-plow [BASQUE ET AL., 1968]. In this model it is assumed that the well-conducting PS has no internal structure (zero-dimensional approximation). It is symmetrical relative to the *z* axis of the system and does not depend on the φ angle, and its motion is described by the trajectory of points on the (*r*, *z*) plane located on the surface of the PS (Fig. 5).

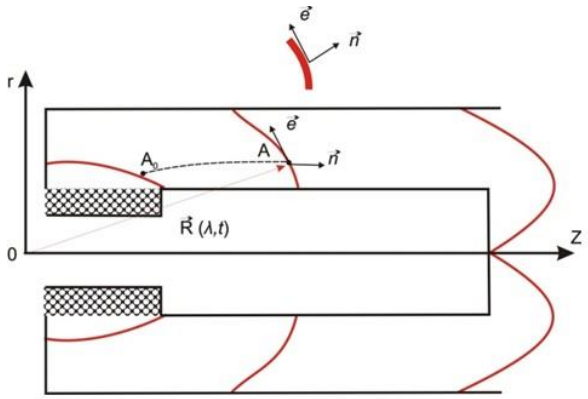

Fig. 5. Coordinate system of the two-dimensional snow plow model. A – point of the electric current sheath defined by coordinate *z* along the layer, A_0 – the initial position of the A point at the insulator,

$\vec{e}_\tau = \frac{\partial \vec{R}}{\partial \lambda} \Big/ \left|\frac{\partial \vec{R}}{\partial \lambda}\right|$ – vector tangent to the layer surface, $\vec{n} = \vec{e}_\tau \times \vec{e}_\varphi$ – normal vector [SCHOLZ, 2016].

For a well operating system, following conditions should be expected [SCHOLZ, 2016]:

- the plasma sheath "sweeps" most of the gas it encounters during the acceleration phase;
- the matching condition expressed by $(U_0^2 C_0^2 / r_A^2 p_0 l^2) \cong \text{const}$ must be fulfilled.

The matching condition, expressed by above formula, combines the parameters of the power source (U_0 – charging voltage and C_0 – capacity of condenser bank), the geometry of the electrode (r_A – radius of the PF anode and l – length of the anode), and the pressure of the working gas p_0.

Radial compression and pinch phase

When the plasma sheath reaches the end of the electrode outlet, it changes the direction of movement from axial to radial, which is due to the appearance of the current density component j_z and thus the magnetic field component B_θ.

The plasma sheath is pushed by the magnetic field pressure and moving towards the electrode axis, forming a funnel-type sheath (Fig. 6).

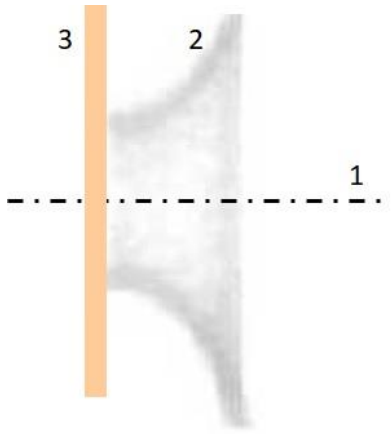

Fig. 6. Image of the plasma sheath taken in visible light using a four-frame camera with an exposure time 1 ns, 1 – the anode axis, 2 – plasma sheath (PS), 3 – the anode plate.

The compression towards the axis is governed by similar rules as in the run-down phase. Movement of the plasma sheath in the radial direction starts with an initial velocity of zero. Then, the layer rapidly accelerates, reaching a radial velocity v_r of several times 10^7 cm/s, before reaches a radius r comparable to its thickness d. The velocity of radial compression v_r can be verified using a streak camera which records the image of the PS in the visible light through a slot (Fig. 7).

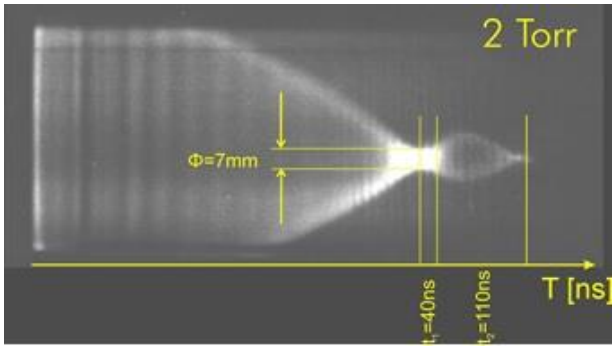

Fig. 7. Image showing the radial movement of the electric current sheath recorded with a fast streak camera in visible light.

The radial compression of the PS lasts from dozens to hundreds of nanoseconds depending on the radius of the anode. For $r < d$, collision of the plasma sheaths must be included in the description of the process. The shape of the PS during radial compression is curved. The radius of the curvature determines the mass outflow, geometry (length), and the pinch plasma parameters.

After the collision of the shock waves of the plasma sheath reaching the electrode axis of the PF system, the pinch phase begins. In this phase of the maximum compression, according to the interferometric data, the electron concentration of plasma reaches the values about $(2 \div 3) \cdot 10^{19}$ cm^{-3} for the minimum pinch radius of the order of 1.5 mm. The same radius of the focus in the soft X-ray is obtained from the camera obscura behind a beryllium filter with a thickness of 50 μm (Fig. 8). At this moment the electron temperature is around 1 keV. However, the neutron emission is negligible in the majority of the PFs as compared to the following phase.

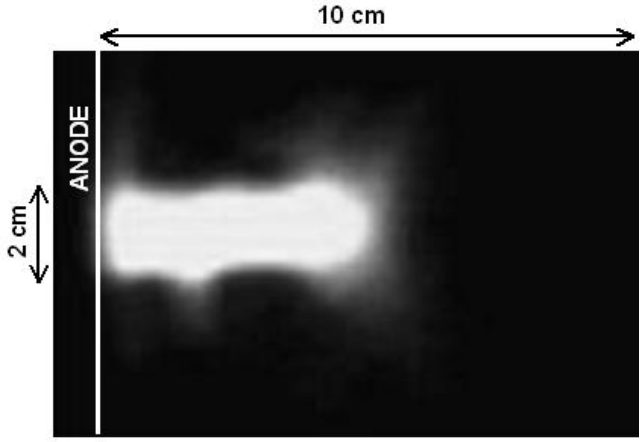

Fig. 8. Image of the plasma focus using an X-ray streak camera in the VUV range (energy of recorded quanta: a window of (0.2 ÷ 0.3) keV and above 0.6 keV), exposure time 2 ns [SCHOLZ, 2008].

Nuclear activity phase

The collision of almost cylindrical plasma sheaths on the PF axis leads to plasma heating and then begins the reverse movement of the plasma. There is the radius of the pinch plasma increase and a respective decrease of electron plasma concentration, and the system switches to the so-called quiet phase which lasts about (20 ÷ 30) ns with a constant radius of the focus. In this phase, the electron plasma concentration decreases at a constant radius. This motion soon stagnates, due to magnetic pressure outside of the plasma, compensating for the expansion momentum. One observes axial movement of the plasma with a very high velocity of about $2 \cdot 10^8$ cm/s. For the PF energy source supply from dozen to hundreds kJ, the plasma column may be about cm in diameter and a few cm long, remaining stable a several dozen ns. After this time, instabilities m=0 begin to develop, leading to necking the plasma column in some places along (Fig. 9), which can be regarded as a re-pinching plasma.

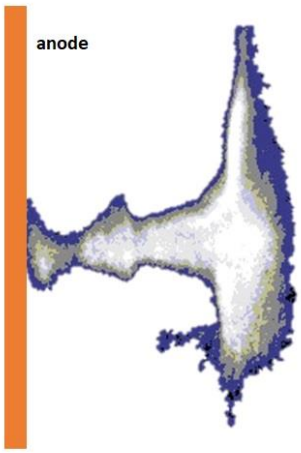

Fig. 9. The VUV image showing unstable m=0 phase of the plasma column taken on four frame camera with time 1 ns shutter during the experiment at PF-24.

In the place of the necking the plasma column breaks and the strong emission of the neutron and hard X-ray pulses accompanies this disruption of the column. At that point, the plasma is characterized by the electron and ion temperatures in the range $T_e \sim (0.3 \div 0.6)$keV, $T_i \sim 1$ keV, respectively and plasma density $n \sim (2 \div 4) \cdot 10^{18}$ cm^{-3}. These parameters do not change significantly for the PF devices operating in the neutron emission optimized mode supply by the PF bank of condensers with the energy from 5 kJ to about 1 MJ [ERHARDT ET AL., 1982].

Measurements of neutron emission from pinch showed that this emission is anisotropic with respect to the pinch, and the spectrum of emitted neutrons reveals immense broadening, which is suggest very high ion temperature in the pinch plasma (40 keV $< T_i <$ 150 keV) [LEHNER, 1970]. This contradicts the actual ionic temperature in the pinch, because the ion temperature of the pinch plasma is low.

It seems that a group of fast deuterons with energies from a dozen to more than a hundred thousand eV, which interacts with the low-energy plasma ions, significantly impacts the fusion.

This phenomena are affected both by the magnetohydrodynamic phase, which is associated to a large extent with the initial conditions of formation and acceleration of the plasma sheath; as well as the phase, which is related to the emergence of phenomena associated with the rapid outflow of plasma from the focus (a decrease in its density) leading to the development of kinetic instabilities.

The mere presence of these fast deuterons does not explain well the amount of the total emission of neutrons from the focus due to the short duration of their confinement in the plasma focus. More probably, is that the source of fusion neutrons is a sort of self - confinement, moderately hot, dense plasma target, with an embedded and trapped ion population of hundreds of keV controlling the fusion rate.

Unfortunately, a complete description of these phenomena does not exist, and the differences in the observed behavior of plasma in the case of different devices is due to the characteristics of these systems, which affect the course of initial phases which form the structure of the plasma sheath, its curvature radius, and kinetic energy.

3. PLASMA FOCUS PF-24 DEVICE IN IFJ PAN

3. 1. DESIGN OF THE PF-24 DEVICE

The PF-24 is the Mather-type device The maximum energy stored in condensers at 40 kV is about 100 kJ and fast current rise time is lower than 2 μs. The PF-24 device consists of the three main units:

- the condenser bank, in which each condenser is equipped with the specially constructed three-electrode spark gap with a trigger electrode,
- the transmission paths, where the connections between the condenser and collector are provided by means of a set of low-inductance cables,
- the experimental chamber with two coaxial electrodes, equipped with a vacuum and gas handling system.

The front view of the PF-24 device in the laboratory hall is show in Fig. 10.

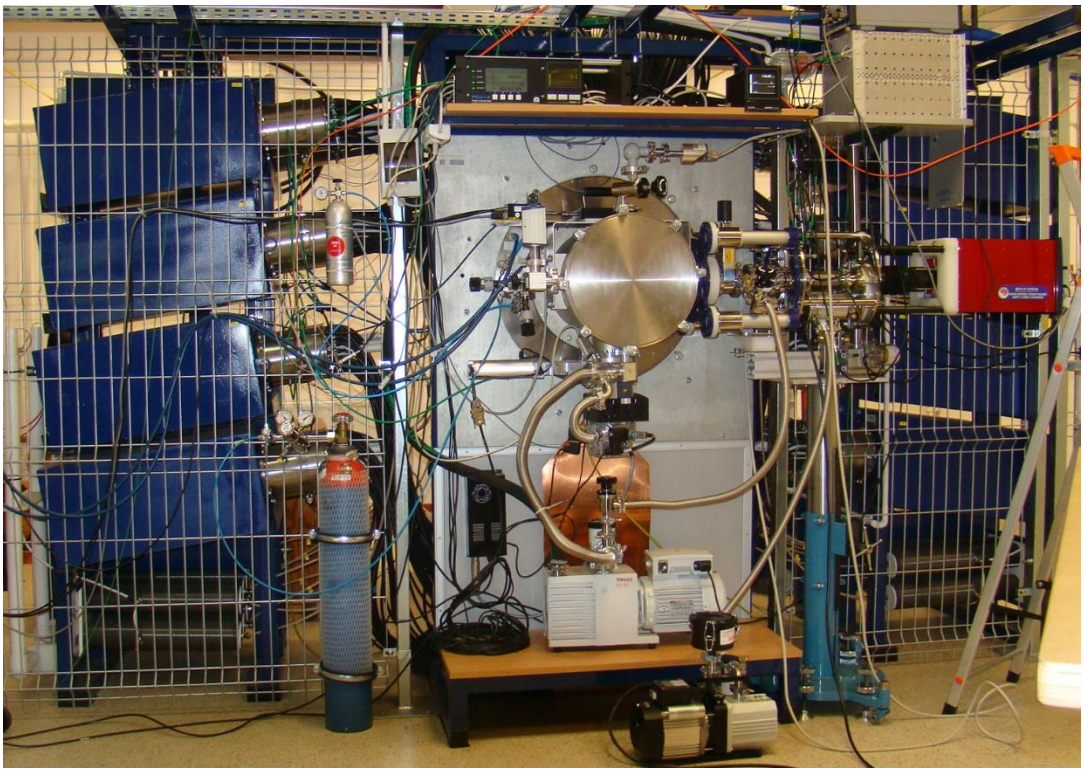

Fig. 10. View of the full set of the PF-24 device in the laboratory hall at IFJ PAN in Kraków.

Condenser Bank and Spark Gaps (IEEE)

The condenser bank of PF-24 consists of 24 pulse condensers (type IK-5/40) connected in parallel through the spark gaps with the anode plate. The condensers have been assembled in the three modules of eight condensers each, placed symmetrically relative to the axis of

the device. (Figs 10, 11) The total capacitance of the condenser bank is 116.12 μF, and it can be charged from 16 kV to 40 kV. It means that the total energy stored in the bank is in the range between 15 kJ and 93 kJ. The inductance of the single capacitor is equal to 40 nH. Thus, the resultant inductance of the battery is equal to L_b = 40 nH/24 = 1.67 nH.

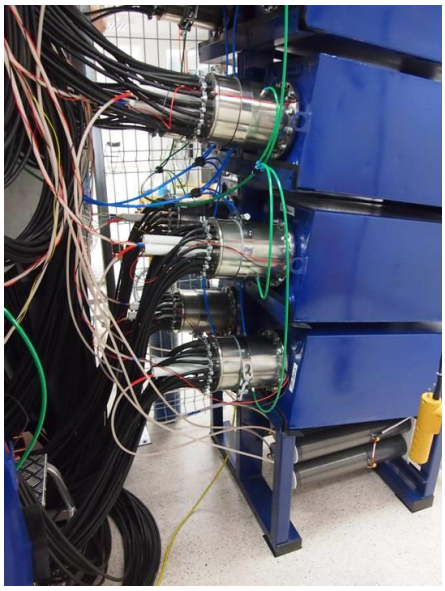

Fig. 11. The PF-24 capacitor bank module with spark gaps.

The spark gap of the field distortion (type IFD-40) has been developed and integrated with the condenser IK-5/40. The integration consists in the use of the condenser's design as a part of the spark gap (see Fig. 12). The shape of the brass rods, being the electrodes of the spark gaps, is shown in Fig. 13. The steering electrode (trigger electrode) made of cooper wire has been placed at 1/3 of the distance from the upper electrode. This type of integrated construction ensures simultaneous energy release from all condensers with jitter up to about 50 ns. The spark gap is sealed that allows operation at gas pressure up to 1.6 bar. The dependence of the breakdown voltage on pressure has a linear character.

The inductance of the single spark gap (L_s) has been determined as 30 nH. Hence, the resultant inductance of all spark gaps is equal to L_s = 30 nH/24 = 1.25 nH.

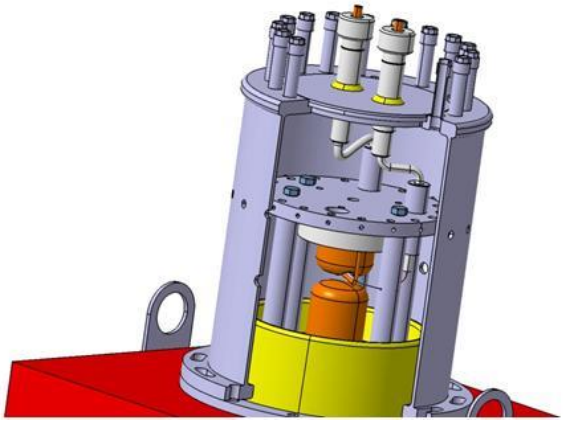

Fig. 12. Connection of the spark gap IFD-40 and the condenser IK-5/40.

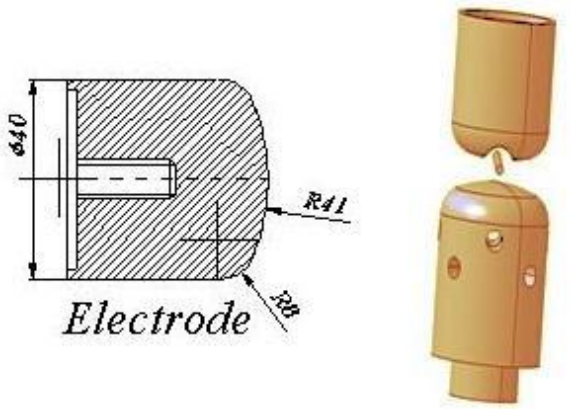

Fig. 13. Profile of the electrodes used for construction of the spark gap IFD-40.

Transmission Path and Collector

The connection of the condensers with the collector was made using a 3.5 m long coaxial wire (type RG 213/U – 2.25/7.25). To reduce the inductance of the transmission path, each condenser was connected by 18 cables grouped in the three modules, six cables each. The resulting inductance of the transmission path is equal to L_t = (3.5 m x 250 nH/m)/(18 x 24) = 2.03 nH.

The collector is made of two parallel stainless steel plates, separated by an insulator (Fig. 14). The first plate has the same electric potential as the anode, and the second as the cathode (common ground). The inductance of the collector was determined at L_c = 2.52 nH.

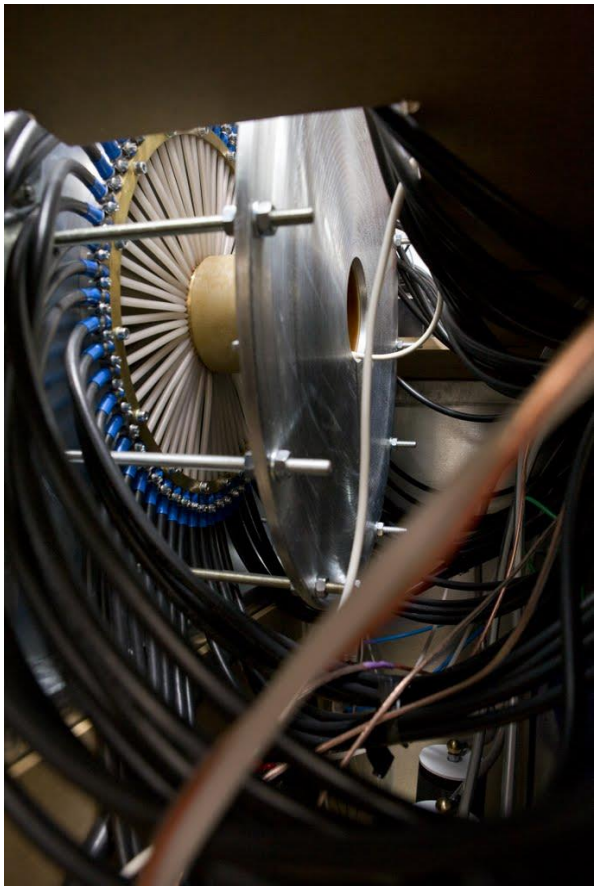

Fig. 14. The PF-24 collector with connection structure. (Foto: Pierzchała)

Experimental Chamber with Electrodes

The experimental chamber is a stainless steel vacuum vessel with a length of 400 mm and a diameter of 320 mm. The pumping system ensures a high vacuum of about 10^{-6} mbar in the chamber. The gas inlet system allows to fill the chamber with various gases and their mixtures.

The PF-24 device has a Mather type of electrode layout inside the experimental chamber (see Fig. 15). The outer electrode (cathode) consists of 16 stainless steel rods, with a length of 174 mm and a diameter of 12 mm each. The reduced cathode radius (i.e. the cathode radius minus the radius of a single rod) is equal to 49 mm. The inner electrode (anode) made of pure anaerobic copper, has a cylindrical shape with a diameter of 62 mm and a length of 250 mm. The effective length of the anode inside the chamber is 170 mm. Both electrodes can be exchanged to another one with a different length (cathode) or a different shape (anode). One of the possible cylindrical electrode's systems with an alternating inductance's anode is presented in Fig. 15. The electrodes are isolated by 60 mm long and 4 mm thick Al_2O_3 insulator placed on the anode. The inductance of the insulator is determined as L_{is} = 1.20 nH.

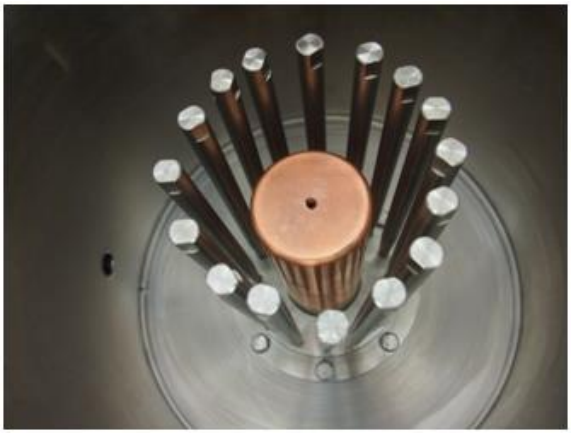

Fig. 15. Electrodes of the PF-24 device. Central copper anode surrounded by a segmented cathode of 16 stainless steel rods.

The schematic diagram of the collector, the vacuum chamber, and the electrodes of the PF-24 device is presented in Fig. 16.

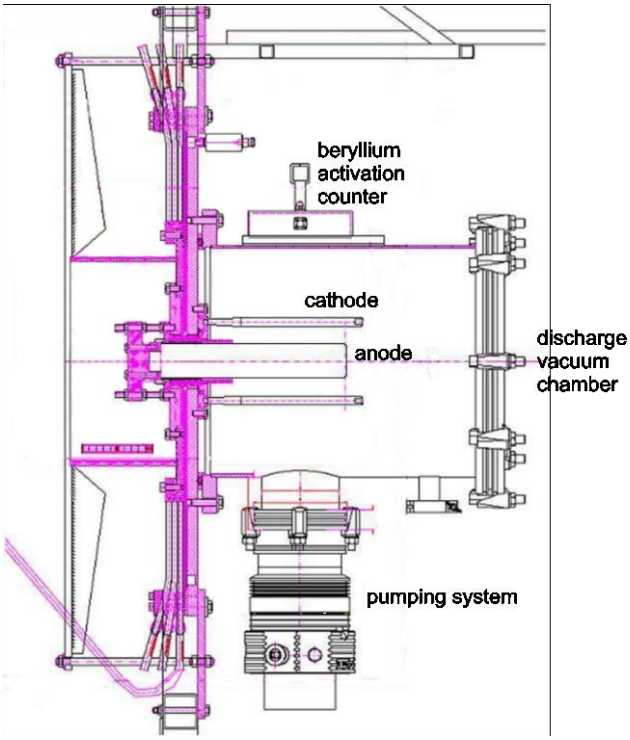

Fig. 16. Scheme of system of the collector, the vacuum chamber, and the electrodes of the PF-24 device seen from side (dimensions have not been preserved).

Total static inductance and resistance of the PF-24 device

The total, nominal, static inductance of PF-24 device considered as the sum of the inductance of all its units L_b, L_s, L_t, L_c and L_{is} is equal to L_0 = 8.66 nH. This result was confirmed with the short-circuit tests connected with damped RLC circuit calculations [MATHER, 1971; BERNARD

ET AL., 1998]. The short-circuit tests were carried out for16 kV of charging voltage and deuterium pressure of 20 mbar and 25 mbar. The calculations based on these tests gave the value of the total inductance L_0 = 8.5 (±3.1) nH and the total, nominal resistance R_0 = 3.1 (±2.3) mΩ [KRÓL, 2015]. Thus, for 17 kV of charging voltage, the quarter period time ($t_{1/4}$) should be equal to about 1.4 μs and short circuit-current ($I_{S\text{-}C}$) should be about 1.5 MA.

3. 2. DIAGNOSTICS EQUIPMENT

Electric probes

The phenomena accompanying the discharge in the plasma focus device can be studied by observing the changes in the current flow in the system. A standard equipment of PF-24 includes the system enables to measure the electrical quantities: total current, voltage and current derivatives. The total current flowing during discharge through the collector is measured by the Rogowski Coil. The Rogowski coil is a type of coreless transformer where the voltage induced in the secondary winding is proportional to the current derivative over time. Thus, by using an electric integrating system configuration the current signal can be obtained.
The calibration factor of the Rogowski coil for PF-24 was determined to 26.4 kA/V.

The voltage into the collector is measured using the capacitive voltage probe mounted between the plates of the collector. The capacitive voltage divider has a limitation at the lower frequencies. Hence, its calibration factor depends on the duration of the pulse. For times less than 1.5 μs this calibration factor is equal to 3.77 kV/V. The derivative over time of the total current is measured with the use of a magnetic probe mounted in the collector.

Neutron counter

For monitoring of the fast neutron emission from the deuterium plasma pinch in the PF-24 device, a beryllium activation counter has been mounted right over the vacuum chamber as shown in Fig. 16. The neutron activation counter operates based on the nuclear reaction and decays: $^{9}Be(n,\alpha)^{6}He \rightarrow {}^{6}Li + \beta^{-}$. The cross section for the $^{9}Be(n,\alpha)^{6}He$ reaction results in a maximum sensitivity to neutrons with energy about 2.5 MeV.

The calibration factor of the counter is equal to $2 \cdot 10^{5}$, and it was established based on the procedure described in [BIEŃKOWSKA ET AL., 2014].

Neutron pinhole camera

An important feature of the neutron source in the PF is its location and evolution in time. The time-resolved neutron pinhole camera, makes use of principles of the optical geometry adopted for neutron imaging, can be used for the investigation of the spatial and temporal distributions of DD neutrons from the PF-24 source [SCHOLZ ET AL., 2014; BIELECKI ET AL., 2015]. An optimization of the pinhole geometry in terms of maximum neutron flux at the imaging plane has been carried out using the MCNP code. The pinhole structure consisting of two copper conical collimators and a cylindrical entrance of 58 mm length enclosed in a polyethylene shield ensure a good collimation of 2.5 MeV neutrons, as well as

effective reduction of thermal neutron current and X-ray contamination [BIELECKI ET AL., 2015].

The total length of camera is 580 mm. The design of the neutron pinhole camera allows imaging a 20 mm long source, emitting neutrons of the order 10^9 neutrons/discharge. Four small-area BCF-12 scintillation detectors (Saint Gobain) in a form of 5 mm x 5 mm x 60 mm rod, each, connected to photomultiplier tube (H3164-10, Hamamatsu) via 25 m long optical fiber serves as a detection system. The time and spatial resolution of about 5 ns and 5 mm, respectively, can be achieved for a line matrix detection system. The traces collected from the scintillation detectors feature signals related to HXR and neutron emissions. During the experiments, the pinhole camera will be placed at the minimum possible distance from the PF-24 chamber, which will ensure the maximum neutron fluency at the imaging plane (see Fig. 17). However, in this case, the time-of-flight method cannot be used to separate the HXR and neutron signals.

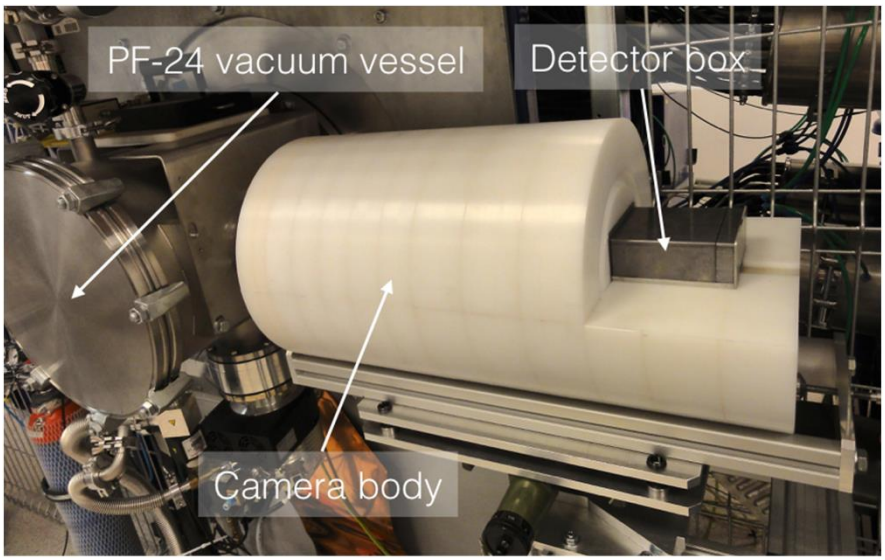

Fig. 17. Neutron pinhole camera [BIELECKI ET AL., 2018].

MCP based, ultra-fast, four frame, SXR and VUV camera

The ultra-fast four-frame soft X-ray (SXR) and vacuum UV (VUV) camera (HS-4F-SXRC) designed and constructed by ACS Company, Warsaw are used in the PF-24 device for imaging of the plasma column and its evolution in time. The main elements of the camera are: pinhole and vacuum track with pumping systems, getable open microchannel plate (MCP) and CCD camera with appropriate optics (Fig. 18). The MCP plays the role of primary detector, radiation amplifier and fast or ultra-fast shutter, while the CCD camera is the final image detector.

The storage (in digital form) of the images of the investigated object appearing on luminescent screens of gated primary image detector. The camera is equipped with four pinholes: two of them of 100 μm in diameter and covered by a 7μm thick Be-filter and two of 50 μm with no blocking foils. The pinholes are placed at 90° to the vertical plane of experimental chamber and a distance of 550 mm from the pinch *z*-axis (see Fig. 18). The

MCP, placed 250 mm behind the pinholes, is divided into four independent quadrants, which enable four frames images with 1.2 ns exposure and 4.7 ns delays between them to be recorded. The delay and exposure time can be adjusted for each quadrant independently. The image magnification factor is equal to 2, and the spatial resolution 230 μm.

From the 2D images of plasma X-ray emissivity, the distribution of electron concentration, temperature, and geometry of plasma column can be obtained.

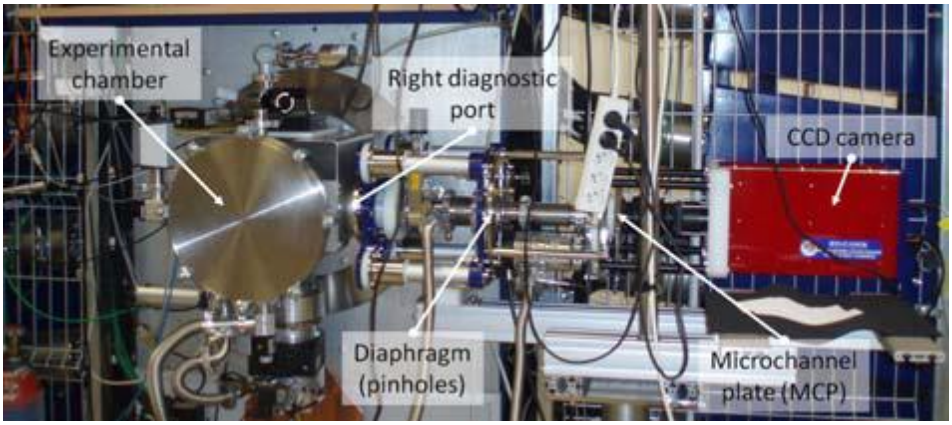

Fig. 18. High-speed four-frame soft X-ray camera with a microchannel plate connected to the PF-24 device [MARCINIAK ET AL., 2016].

3. 3. MEASUREMENTS OF THE CURRENT GENERATOR'S PARAMETERS OF THE PF-24 DEVICE

To define the current generator's exploitation possibilities of Plasma Focus device, the internal parameters of the generator such as an inductance L_0 and a resistance R_0 have been determined by measuring the current in the short-circuit regime.

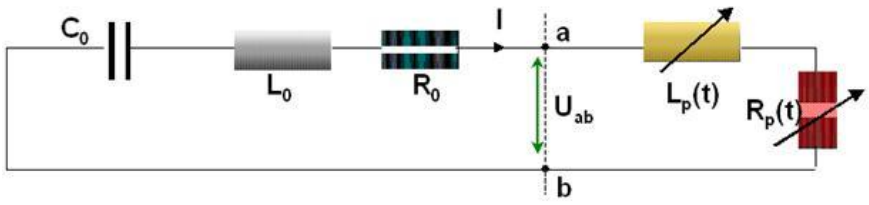

Fig. 19. The equivalent circuit for a discharge in Plasma-Focus. U_{ab} is voltage between the electrodes. C_0, L_0, R_0, is capacity, inductance and resistance of the power source, respectively. L_p is inductance connected with the motion of current layer and R_p is ohmic plasma resistance [SCHOLZ, 2016].

The equivalent electrical circuit of the PF-24 device [SCHOLZ, 2016] is shown in Fig. 19. The electrical parameters (current and voltage) in such a circuit can be described by the expression:

$$U_0 - \frac{1}{C_0}\int Idt - L_0\frac{dI}{dt} + R_0 I = U_{ab}(t).$$

Where: U_{ab} is the voltage between electrodes, I is the discharge current, R_0 and L_0 are the internal resistance and inductance, respectively. C_0 is the capacity of the condenser bank, and U_0 is the charging voltage of the bank. L_0 is a sum of the inductance of the collector and the node's, anode–insulator inductance. From this formula L_0 and R_0 can be determined for $U_{ab} = 0$.

To simulate the short circuit ($U_{ab} = 0$), the measurements have been performed at the pressure of 25 mbar of deuterium in the chamber. In these conditions an electric discharge occurred in one current channel near the insulator. The initial charging voltage was set to U_0 = 16 kV. A representative result of the measurements is shown in Fig. 20. From this function the damping coefficient (α/ω) and the oscillation period T has been defined. Hence, the quarter discharge time $T_{1/4} \cong 1.8$ μs, the nominal inductance $L_0 \cong 11$ nH, and the resistance $R_0 \cong 1.4$ mΩ have been determined. The total neutron emission (Y_n) from the DD reaction that depends on the energy W_0 of the capacitors bank (given in kJ), can be expressed by the formula $Y_n \sim 10^7 W_0^2$ [MICHEL ET AL., 1974]. Since, the expected capability of the maximal neutron yield for PF-24 is about 10^{10} neutrons per discharge.

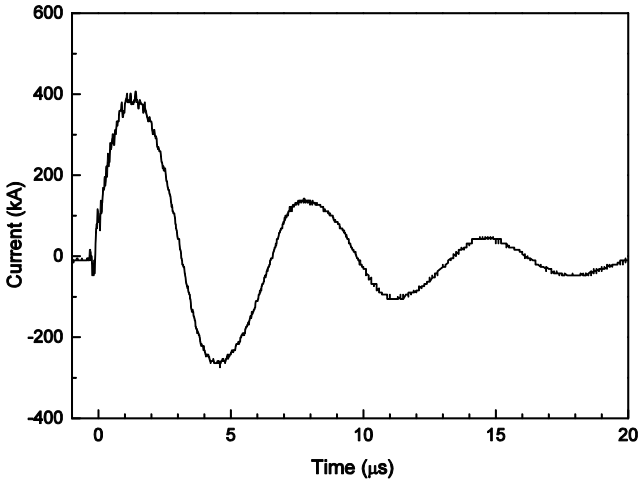

Fig. 20. The current waveform of the PF-24 short circuit experiments.

4. THE MAIN AIMS of STUDIES, RESULTS and PERSPECTIVES

4. 1. NEUTRON EMISSION MEASUREMENTS

Based on: [MARCINIAK ET AL., 2018]

The total neutron yield is measured for each discharge using the neutron activation counter as described in chapter 3.2. The total number of over 2000 discharges was performed at very wide pressure range between 1.5 mbar and 17 mbar of deuterium during the operation time of PF-24 since 2014. The analysis of the neutron emission dependence on the D_2 pressure was reported in [MARCINIAK ET AL., 2018]. The distribution of measured neutron yield Y_n for 413 discharges done for 17 kV charging voltage and at the range between 2 mbar and 5 mbar of deuterium is presented in Fig. 21. The median, average and maximum Y_n value for these 413 discharges is equal to $(2.6 \pm 0.2) \times 10^9$ n/discharge, $(4.5 \pm 0.1) \times 10^9$ n/discharge, and $(1.89 \pm 0.04) \times 10^{10}$ n/discharge, respectively.

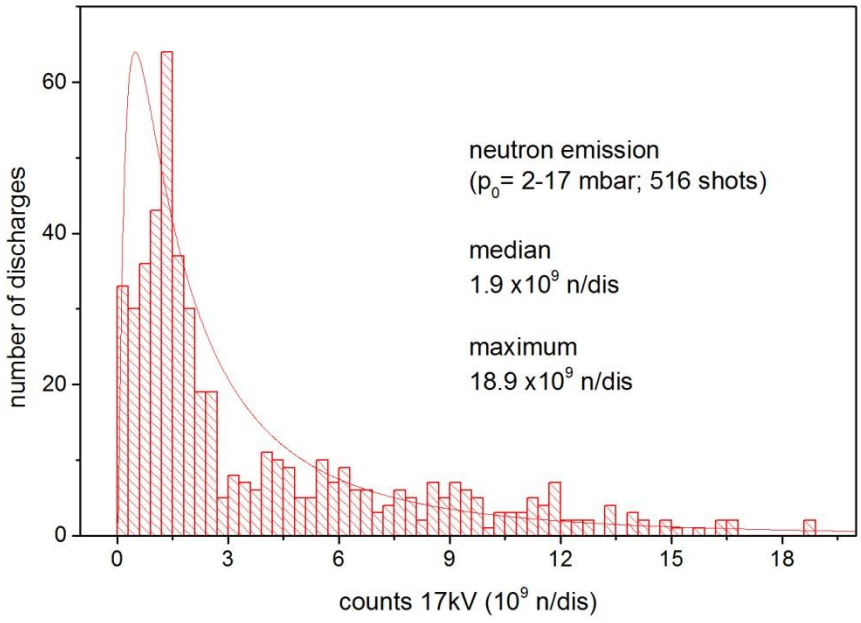

Fig. 21. Distribution of the measured total neutron yield (Y_n) for 516 discharges in the range from 2 mbar to 17 mbar of initial D_2 pressure (p_0).

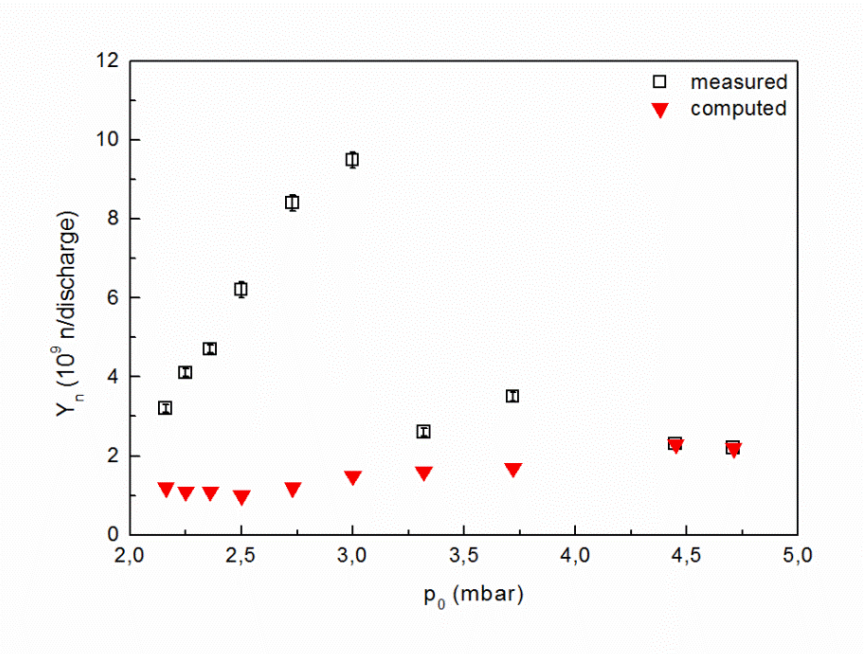

Fig. 22. The measured and computed total neutron yield (Y_n) versus initial D_2 filling pressure (p_0) [MARCINIAK ET AL., 2018].

The measured Y_n values, represent an average of 10 to 100 discharges for a given gas pressure and the total neutron yield computed using the Lee model configured to the PF-24 device [LEE, 2018; LEE, 2014], are shown in Fig. 22. A strong non-monotonic dependency of the measured Y_n on the pressure (p_0) was observed in the investigated range of pressures. The inconsistency of the measured and computed neutron output near the maximum emission is particularly significant (see Fig. 22). Moreover, the calculated neutron yield using the Lee model code differs from the measured values for the high neutron yield (above median value) for all simulated discharges. On the other hand, for the neutron output below median value computations are in good agreement with the experimental values. In this case the measured Y_n has been reproducible by the model for 73% of fitted discharges (relative errors smaller than 6 %). It should be mentioned that discharges with Y_n higher than 2.6×10^9 n/discharge were achieved in 56 % of discharges for $p_0 \sim 3$ mbar and only in 19 % of discharges for $p_0 > 3$ mbar.

Comparison of the measured and computed yield Y_n versus pressure using the Lee model code indicated, that the character of neutron emission from the deuterium plasma focus is more complicated than the beam-target neutron generating mechanism used in the code [LEE AND SAW, 2008A; 2008B]. After comparing many Plasma-Focus devices, it turns out that PF-24 works significantly more efficiently (on average 2–3 times higher Y_n values) than the previously studied devices (at given bank, tube and operational parameters). Hence, the PF-24 device has an optimized configuration for the DD fusion neutron emission [MARCINIAK ET AL., 2018; AKEL ET AL., 2019]

4.2. RADIATIVE COLLAPSE

Based mainly on: [Marciniak, 2020; Marciniak et al., 2020]

In Plasma-Focus discharge the current flows through plasma in the z axis direction and compressed it due to the self-generated magnetic field pressure and the Ampere's force (or the Lorene force) [LIBERMAN ET AL., 1999; HAINES, 2011; SADOWSKI AND SCHOLZ, 2012]. The created plasma pinch is an efficient source of electromagnetic radiation (i.e. VUV and SXR). Assuming that the pinch is in equilibrium, i.e. the internal plasma pressure is balanced by the external magnetic field pressure, and the total bremsstrahlung radiation power is balanced by the total power of Ohmic heating (during pinch life), then the current flowing through the pinch reaches the characteristic value for a given gas, so-called Pease-Braginski current (P-B current) [SHEARER, 1976; LIBERMAN ET AL., 1999; HAINES, 2011].

The 113 discharges were carried in D_2 and [(100%-x)D_2–xAr] mixtures with Ar fraction x in the range between 3% and 60 %. The PF-24 were operated with 17 kV charging voltage under constant total initial pressure of about 2.9 mbar. Each experimental discharge was simulated individually using the enhanced 5-phase Lee model code enabling computation in gas mixtures. The Lee model code is a relatively simple, efficient, hybrid code, based on the 0/1-dimensional snow-plough and elongated slug model of the plasma sheet-shock structure movement, simulating all main phases of discharge (5-phase or 6-phase code) in a plasma-focus [LEE, 2014; LEE AND SAW, 2017]. The registered experimental discharge current was fitted with the computed discharge current using 4 model parameters and 2 operation parameters of PF device. The model parameters represent the percentage of mass sweeping by the magnetic piston structure in reference to the total mass/density of gas between and in front of electrodes, axial (f_m) and radial (f_{mr}) phases of discharge, respectively and the percentage of current flowing through the plasma sheet-shock structure in reference to the total current flowing between the electrodes in axial (f_c) and radial (f_{cr}) phases of discharge. More detailed information about the Lee model code can be found in Refs. [LEE, 2014; AKEL ET AL., 2019; LEE AND SAW, 2017]. The measured and computed parameters of plasma/discharge were obtained for these 113 discharges. Based on them, the radiative compression parameters and indicators: total X-ray line yield, (total/effective) atomic number, initial pinch: radius, ion number density and ion temperature were determined for [(100%-x)D_2–xAr] mixture [MARCINIAK, 2020].

The measured and computed current parameters: maximum $\langle I_{max} \rangle$ and pinch $\langle I_{pp} \rangle$ current; are show in Fig. 23. The P-B current $\langle I_{P-B}^{comp} \rangle$, the reduced P-B current $\langle I_{P-Breduced}^{comp} \rangle$, which includes the line and recombination radiation occurring in the case of gases with higher Z or gas mixtures) and the plasma pinch current $\langle I_{pp}^{comp} \rangle$, which flows through plasma column) were computed at time t, when the reduced P-B current achieved its smallest value during pinch lifetime [MARCINIAK, 2020; MARCINIAK ET AL., 2020].

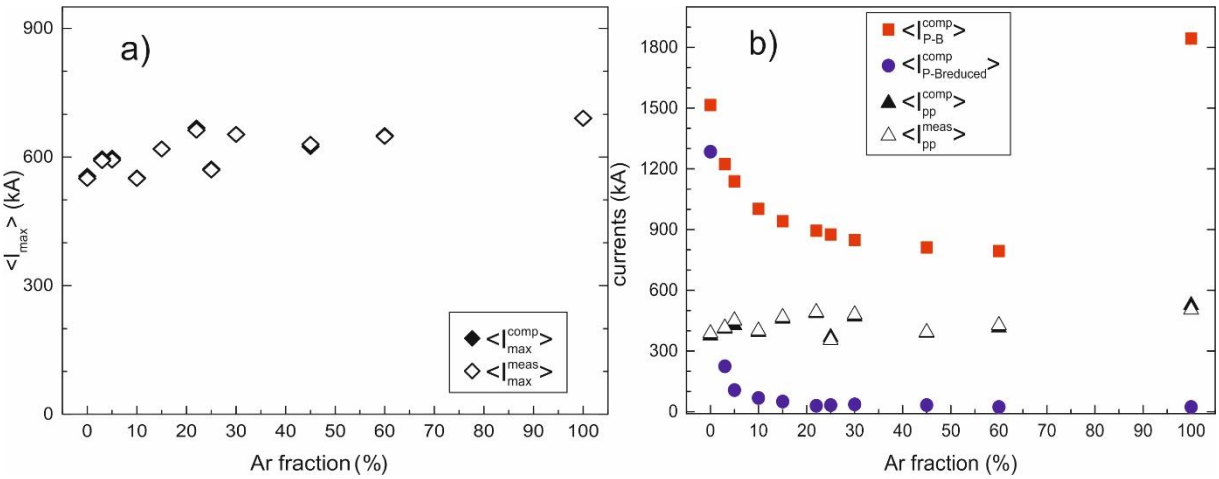

Fig. 23. The average values of (a) measured $\langle I_{max}^{meas} \rangle$ and computed $\langle I_{max}^{comp} \rangle$ maximum current; (b) measured $\langle I_{pp}^{meas} \rangle$ and computed $\langle I_{pp}^{comp} \rangle$ pinch current and the $\langle I_{P-B}^{comp} \rangle$ and $\langle I_{P-Breduced}^{comp} \rangle$ currents versus Ar fraction in [(100%-*x*)D_2–*x*Ar] mixture. [MARCINIAK, 2020]

The $\langle I_{P-Breduced}^{comp} \rangle$ decreases with increase of Ar fraction *x*. Both, the maximum and pinch current values exceed the $\langle I_{P-Breduced}^{comp} \rangle$ value significantly for *x* > 5%.

The analysis of other radiative compression parameters has shown that increase of the total/effective atomic number of gas mixtures increases the probability of occurrence of the plasma radiation compression. The relatively weak radiative compression was found for some discharges for *x* = (15–60) % Ar, while the relatively strong radiative compression was only present in pure Ar. This was caused by to too low total x-ray line radiation emission during pinch lifetime due to specific changes in the electro-dynamics of plasma/discharge prior to the plasma pinch formation [MARCINIAK, 2020].

4.3. BCF-12 DETECTORS TEST

Based on: [BIELECKI ET AL., 2018]

This work was dedicated to study of the efficiency of the small-area BCF-12 detectors dedicated for the neutron pinhole camera. The knowledge of the efficiency and general performance of the detectors is crucial for the determination of the spatial distribution of neutrons emitted from plasma column created in Plasma-Focus device. In turn, the spatial distribution of this neutron emission allows on understanding of the fusion reaction character in a plasma pinch.

For this purpose, small-area detectors based on BCF-12 scintillation rods and Hamamatsu photomultiplier tubes (PMTs) were designed and constructed. The main feature of these detectors was to separate the scintillation element from the PMT in order to avoid an influence of the electromagnetic noise on with the PMT and data acquisition system, which is produced

during a Plasma-Focus discharge. In addition, this design of the detector allows for a more optimal development of the neutron pinhole camera.

Two connecting technique of the scintillation element with optical fiber in these neutron detectors were explored (Fig. 24).

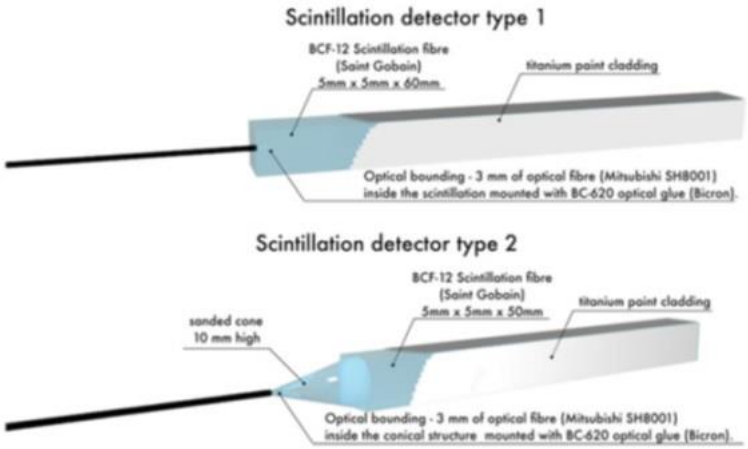

Fig.24. The construction details of the two types of scintillation detectors.

In order to determine the efficiency and general performance of the pinhole camera detectors, the experimental investigations using a neutron generator and a Pu–Be source were combined with MC computations using the Geant4 code for these two type of the BCF-12 neutron detector. Then, this detectors were tested on the PF-24 device.

The BCF-12 scintillators (Saint-Gobain Crystals, France) dedicated as detection elements for neutrons detectors, which plan to use in the pinhole camera, have a form of (5×5×60) mm rods. These scintillators have the trapping efficiency, determined by refractive indices of the core (1.60) and cladding as well as the cross section of the scintillator, permits the collection of <4% of the photons during passage down the scintillator. The collected light is transported *via* 25 m long fiber optics to the PMTs and data acquisition (DAQ) (see Fig. 25).

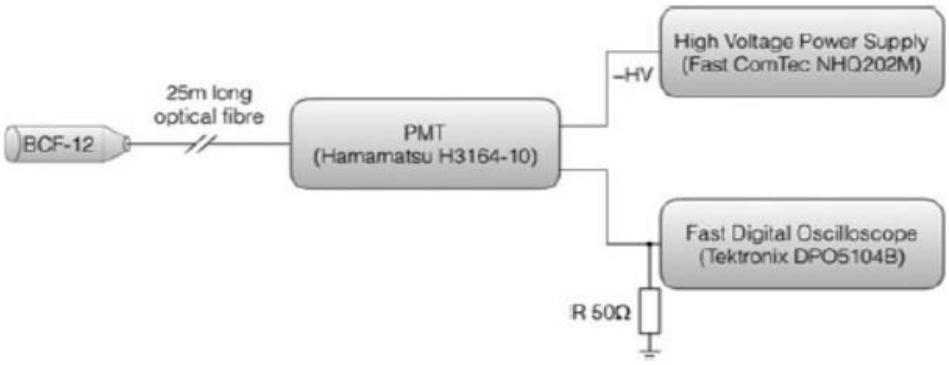

Fig.25. Block diagram of the setup used to determine the efficiency of the scintillation detectors.

As mentioned before the two experiments were performed for determination the efficiency of detectors. First was performed with Pu-Be source with a neutron yield of 5.3×10^5 n/s and then with neutron generator (NG). The neutron yield from NG was monitored by a BCF-720 probe (1.6% efficiency at 19 MeV) and was ~1×10^4 n/s during the experiment.

Efficiency of the detectors was investigated by means of Geant4 (version 9.3.p02) computations (Table 1). Two kinds of calculations related to the experiments were performed:

- modeling of detection of neutrons emitted from the Pu–Be source
- modeling of 14.1 and 2.45 MeV neutron detection with the neutron generator.

The BCF-12 models related to both types of detectors' geometry shown in Fig. 24 were constructed. To estimate the efficiency of the detectors, a custom-made routine has been developed that counts photons generated and transported to the optical fiber.

Table 1. The results of the experimental and Monte Carlo determination of the BCF-12 detectors efficiency.

Detection efficiency [%]				Source (Energy)
Calculated		Experimental		
Type 1	Type 2	Type 1	Type 2	
0.49 ± 0.08	0.51 ± 0.06	0.19 ± 0.06[a]	0.29 ± 0.09[a]	NG (2.45 MeV)
1.6 ± 0.1	1.7 ± 0.1	0.53 ± 0.14[a]	0.59 ± 0.14[a]	NG (14.1 MeV)
0.9 ± 0.04	0.94 ± 0.05	0.90 ± 0.06	0.93 ± 0.05	PuBe

[a] High experimental uncertainty due to low efficiency of the reference probe.

The calculated efficiency of 2.5 MeV neutrons detection is ~0.5% for both types of the detectors, while the experimental values are ~50% lower the calculated ones. However, the experimental results feature high measurement uncertainties. For detection of 14.1 MeV neutrons, the calculated efficiency is around 1.5% for both types of the detector, while the experimental results give ~0.5% for both types of the detectors. As previous, the experimental results feature quite high measurement uncertainty.

The experimental and computational results of efficiency determination for the detection of neutrons from Pu–Be source are consistent. In this case, the efficiency is ~0.9%. The experimental uncertainty is much lower in this case due to the precise knowledge of the source activity.

In order to test the detectors capability of the radiation detection with PF-24 source were performed several experiments. Fig.26 shows an example of X-ray and neutron time traces collected by BCF-12 detectors during the PF-24 discharge.

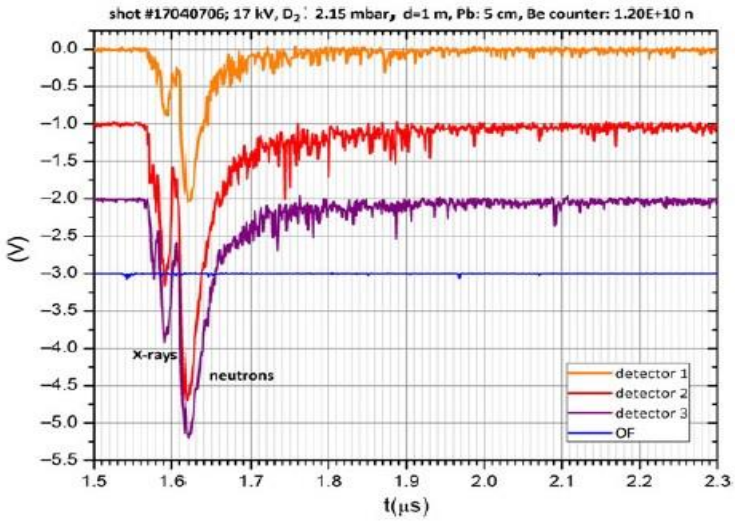

Fig.26. The X-ray and neutron time traces collected using BCF-12 detectors for a PF-24 discharge.

Two types of small-area BCF-12 scintillation detectors have been studied in order to determine the detection efficiency. There is no statistically significant difference in efficiency of the two types of detectors. However, the trend shows that possibly the second approach to the construction is more efficient. The discrepancies between experimental and Monte Carlo simulation results are caused by high uncertainties of the experimental results as well as by the simplified model of the detectors in Monte Carlo calculations. Additionally, from experiments on PF-24 one can see, that the plastic optical fiber connecting scintillator with PMT gives a signal from the X-ray radiation. It means, that this kind of the optical fibers should be exchanged into the quartz ones to eliminate the contribution from X-ray.

4.4. Proton – boron nuclear reaction in Plasma-Focus device

Based on: [Scholz et al., 2019]

The deuterium-tritium (d-t) fusion reaction is foreseen as the main reaction in future controlled thermonuclear reactors in order to produce electricity. This reaction was chosen because of its high thermal reaction rate at relatively low temperatures about 10 -20 keV in comparison with reactions of other light nuclei.

The (d-t) fuel cycle presents two major challenges for reactor designers:

1. the 14 MeV neutrons produced in the t(d,n)α reaction;
2. the presence of tritium in the fuel cycle.

A huge stream of 14 MeV neutrons causes:

- damage reactor components (principally the structure of the blanket and shield) thereby limiting their useful lifetime; activate materials, thereby opening the possibility that (d-t) fusion reactors will produce large volumes of radioactive wastes.

In addition, the presence of tritium in the fuel cycle causes, that following problems should be solving

- Tritium must be bred through the reaction n(^{6}Li,t)α in a breeding blanket which surrounds the plasma.
- Breeding of tritium can result in large onsite tritium inventories (principally in the blanket and tritium recovery system) raising both safety and nuclear proliferation concerns.

Therefore, the motivation for studying alternative fuel cycles for fusion can be summarized as follows; firstly, tritium should be removed from the fuel cycle to simplify this cycle (without tritium cultivation) and thus solve nuclear proliferation problems; secondly, eliminating (or greatly reducing) neutron production in fusion reactors as a means of avoiding (or greatly ameliorating) neutron damage to, and activation of fusion reactor components.

Such problems can be solved by using aneutronic nuclear reactions that produce much less high-energy neutron radiation. One example of such a reaction in which neutron generation is almost absent is the fusion reaction between proton (p) and boron (^{11}B) nuclei. Here, the energy is released as the kinetic energy of alpha particles rather than neutrons. Furthermore, the maximum of the ^{11}B(p, α)αα cross section of 1.2 barns occurs at 600 keV in the center of mass and it is higher than d(t,n)^{4}He cross section for this energy. However, the main difficulty for (p^{11}B) fusion is actually related to the high ion temperatures needed to achieve this high reactivity. In this way, for plasma in thermal equilibrium, the electron temperature is also very high, which means that the power of radiation losses due to bremsstrahlung is very high. Thus, radiation losses prevents ignition in (p^{11}B) fuel [MOREAU, 1977].

It seems that this problem can be overcome by carrying out this reaction in conditions far from thermal equilibrium. Thus, various schemes were considered to implement controlled thermonuclear fusion based on the ^{11}B(p, α)αα reaction.

One of such systems where the fusion reaction between hydrogen and boron nuclei could be carried out in conditions far from thermal equilibrium is the Plasma-Focus device (PF). So, to trigger this reaction in the PF, one need to create a pinch of hydrogen boron plasma, maintaining the standard operating conditions of the PF device. This can be achieved by adding boron to the PF system at an appropriately selected time, in such a way as not to disturb the formation and acceleration phase of the plasma layer in the system. A good solution to this problem seems to be to separate the last clamping phase of the PF discharge from the forming and acceleration phase. However, it should be remembered that during the PF discharge, the linear density of the added boron should be limited so that it can be to obtain a well-compressed pinch plasma column with hydrogen and boron ions. Considering that, we propose to use laser ablation from the boron sample, which is placed in the selected area of the PF anode. This method allows obtaining a boron plume near the anode axis of PF

during imploding of hydrogen current sheath in the PF device. Then in turn allows obtaining a boron-hydrogen pinch plasma column. Thus, one can expect that in the PF conditions, the fusion reaction of hydrogen and boron nuclei will take place.

The scheme of the proposed experiment for generating dense and high-temperature boron-hydrogen plasma in the PF device is shown in Fig. 27.

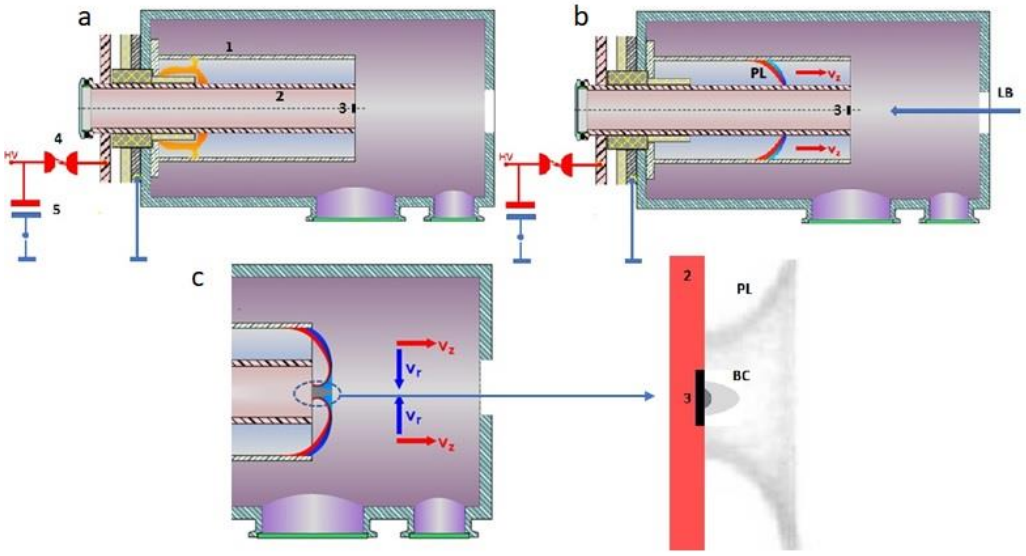

Fig.27. The laser ablation experiment in PF-24 device. a) phase of the breakdown and hydrogen plasma layer (PL) formation, b) phase of the run-down (acceleration of PL) and moment of laser beam (LB) interaction with target , c) phase of the radial compression of PL and free expansion of the boron plasma cloud (BC). 1 –cathode of PF device, 2 –anode of PF, 3 – boron target, 4 – spark gaps, 5 – condenser bank.

In order to carry out such an experiment, the following issues should be determined:

- whether the laser used may cause self-breakdown of the working gas in the PF chamber in front of the sample;
- measurement of ablated mass in this experiment M_a;
- estimation of the (N_H/N_i) and $\left(n_{plH}/n_{pli}\right)$ and dimension of boron plume

where: N_H, N_i are linear density of hydrogen and boron ions, respectively; n_{plH}/n_{pli} is the hydrogen to boron plasma density ratio.

Before the main proton-boron experiment boron ablation using a A Nd:YAG laser (Lotis TII, LS-2147) has been measured. The laser beam used in the experiment had the following parameters: Gaussian profile, pulse duration 18 ns, wavelength 1064 nm and diameter 8 mm.

Two series of experiments were carried out. The first for verify deuterium self-breakdown with a laser beam in the pressure range of 1 ÷ 3 mbar and the second for estimate quantity of ablated mass. Firstly, during the first series no the hydrogen self-breakdown in the chamber was found in this pressure range. Secondly, a crater due to ablation appeared regularly on the target in the place of the focused laser beam (see Fig. 28)

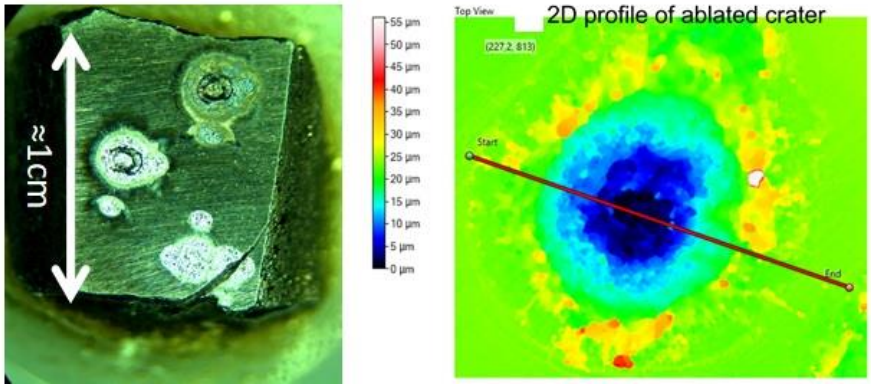

Fig.28. The picture of the craters and 2D profile of the crater created in the boron sample after ten laser pulses (707 mJ).

A summary of the results of the experiment and estimations based on a simple model for one laser shot with 707 mJ energy is shown in Table 2.

Table 2. Laser ablation of boron sample.

	S_f – laser spot [μm^2]	M_a – total ablated mass [µg]
Experimental results	$2.83 \cdot 10^5$	0.7 (±0.4)
Calculation results	$2.83 \cdot 10^5$	2.97

To estimate the size and the density of a boron cloud plasma one should include and describe processes of the boron cloud formation. During the laser nanosecond pulse the following processes take place:

- absorption of the laser energy in the sample;
- conductivity of band electrons during absorption;
- thermal conductivity and electron-lattice collisions.

Finally, the laser beam with a several-nanosecond pulse heaths the sample and then produces a vapor-plasma cloud on the sample surface which is located on the anode of the PF device (see Fig. 29).

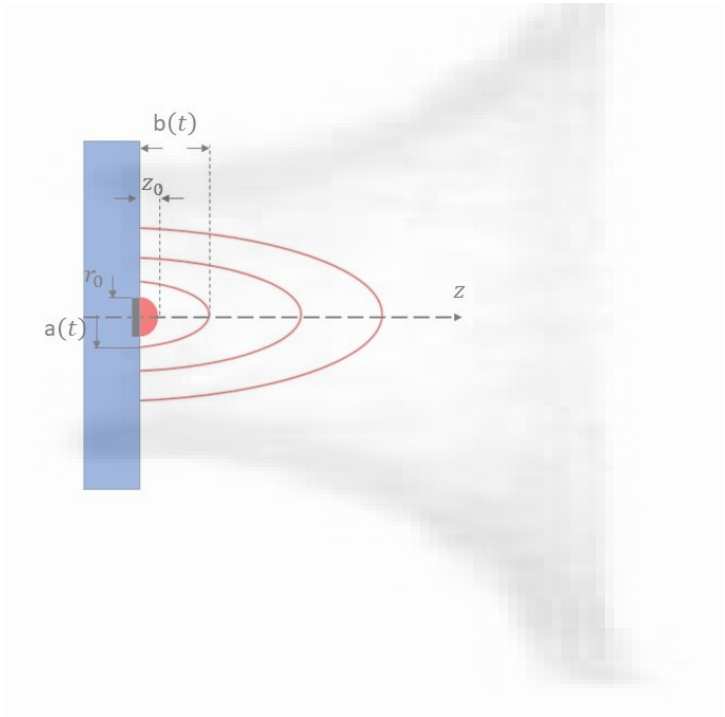

Fig.29. Diagram of boron plasma cloud expansion from a sample placed in the PF anode, relative to the location of the hydrogen plasma layer

Based on the model presented in the paper [ANISIMOV ET AL., 1993] the estimation of the dimensions of the boron plasma cloud were done, for $\kappa = c_p/c_v = 5/3$, using the formulas:

$$b(t) = r_0\sqrt{3\left(\frac{t}{t_0}\right)^2 + \left(\frac{z_0}{r_0}\right)^2 + 2}\ ,\ \ a(t) = \frac{b(t)}{\sqrt{2}}.$$

The initial radius of the cloud r_0 can be approximated by the radius of the laser spot. The height of the cloud in the z-direction is about $z_0 = v_s\tau$, where v_s is the velocity of sound and τ is the laser pulse duration. In our experiments typical value of the $r_0 \cong 500$ μm are obtained (see Fig.29). The characteristic time scale for expansion is $t_0 = \frac{r_0}{\sqrt{(5\kappa-3)E/M_a}}$, where E – the initial energy of the plasma plume and M_a is the ablated mass during laser shot.

Assuming that the plasma cloud has elliptical symmetry, the volume of this cloud is $V(t) = \frac{2}{3}\pi a^2(t)b(t)$, so the density of boron ions uniformly distributed is as follows: $n_{0B} = N_A\frac{M_a}{M_m V(t)}$.

Where: N_A – Avogadro number, M_m – molar mass of boron, M_a – mass of ablated boron, $V(t)$– volume of plasma cloud at time t.

Figs 30 and 31 show the n_{0B}/n_{0H} ratio dependent on t_0 for two different working gas pressures and the change in time of the dimensions of the plasma cloud in the radial and axial direction, with respect to the anode face of the PF-24. Shown in in these figures dependencies were obtained for $M_a = 0.7$ μg, the laser energy E = 707 mJ, $r_0 \cong 500$ μm and the initial plasma temperature T = 1eV.

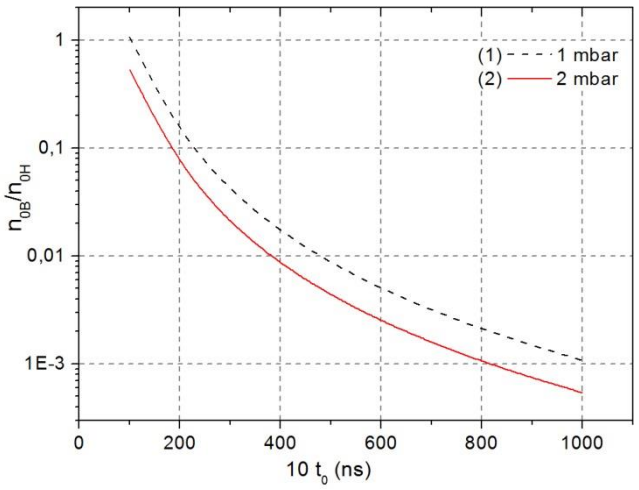

Fig. 30. Ratio n_{0B}/n_{0H} for different hydrogen pressures: (1) dashed line: 1 mbar, (2) solid line: 2 mbar.

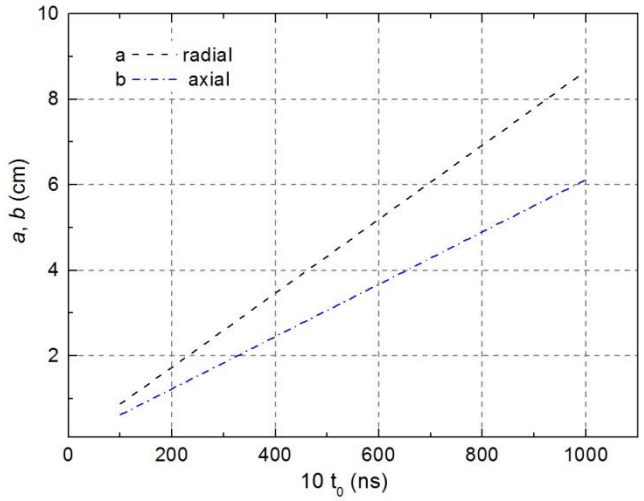

Fig.31. Radial (a) and axial (b) dimensions of the plasma cloud for hydrogen pressure 1 mbar and $M_a = 1.2$ μm.

Here n_{0H} depends on the initial pressure of hydrogen filling the PF-24 vacuum chamber, and n_{0B} on the ablated boron mass from the sample, depending on the laser energy and the characteristic expansion time t_0.

The knowledge of time t_0 and plasma cloud expansion conditions allows to determine the synchronization between the moment of laser ablation completion and the time of plasma sheath compression in the PF-24 device. It means that in real experiment one should correlate the creation of boron plasma cloud with evolution of the PF-24 discharge as shown on Fig.32. Appropriate selection of the time to start boron ablation will determine ratio n_{0B}/n_{0H} for a given hydrogen pressure in the vacuum chamber of PF-24.

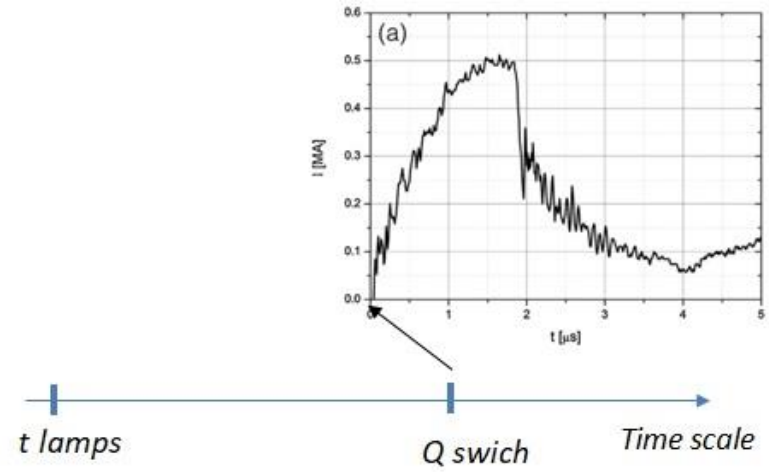

Fig.32. Scheme of the correlation between laser and the evolution of discharges in PF-24.

One can summarizing above consideration as follows:

- Estimation of the dynamics of the plasma cloud expansion caused by ablation gives the possibility of correlating the moment of laser beam generation with the time course of acceleration and plasma sheath compression in the PF-24 system.
- Based on this one can elaborate the model of the alpha particle yield for $^{11}B(p, \alpha)\alpha\alpha$ nuclear reactions based on the measured electrical parameters (current, current derivative, the voltage on the probe) of the PF-24 system. This enables rough experimental verification of assumptions and approximations in the developed models.

5. PROPOSED OF PHD THESIS

5.1 THE PHENOMENON OF RADIATION COMPRESSION IN THE GAS MIXTURES FOR THE PF-24 DEVICE

The plasma focus PF-24 device is a dynamic, non-cylindrical, Z-pinch plasma generator with an experimental chamber of the Mather type. Plasma is created in a working gas as a thin, radially symmetrical current layer formed as a result of an electric leakage on the insulator surface between coaxial electrodes. The current layer rapidly detaches itself from the insulator and is accelerated along the anode with the Ampere force. The current sheath is compressed at the end of anode and so-called plasma pinch is created. The physical processes occurring during discharge in the plasma-focus device are still not fully explored and understood. One of such phenomenon is the plasma radiation compression. In this process, the plasma density and X-ray emission should increase significantly, while the plasma volume and its temperature should decrease significantly.

In the frame of thesis, the studies of the plasma radiation compression in gas mixtures taking place during discharge in a plasma focus device will be carried out. The works will be based on experiments performed using the PF-24 device and on the theoretical calculations.

Evaluation and analysis of the experimental data obtained using different diagnostics including: Rogowski coil, magnetic probe, ultrafast 4-frame imaging system in vacuum ultraviolet and soft X-ray; will be completed with the simulations and calculations using the Lee model code.

The obtained results will provide a set of parameters describing the plasma and discharge as a function of time. They will allow to determine the occurrence of the phenomenon of plasma radiation compression and to determine the conditions of its development during the discharge. In addition, the results will be used to verify the Lee model code for gas mixtures. An important part of the work will be cooperation with the author of the code (Prof. S. Lee) in the process of its verification, modification and further development.

5.2 The study of the proton boron (pB) reaction rate in the Plasma-Focus device.

The deuterium-tritium fusion reaction is foreseen as the main reaction in future controlled thermonuclear reactors in order to harvest energy. This applies to both thermonuclear fusion research based on magnetic and inertial confinement of the plasma fuel near steady-state conditions. This reaction was chosen because of its high thermal reaction rate at relatively low temperatures about 20 keV in comparison with reactions of other light nuclei. However, a serious disadvantage of this reaction is that it is accompanied by intense high-energy neutron flux. This makes it necessary to use a thick, sophisticated blanket around the plasma as a fuel increasing considerably the size of the fusion reactor. In addition, radioactive waste is generated and tritium breeding is necessary.

Such problems can be overcome by driving the aneutronic nuclear reactions that produce substantially less high-energy radiation. An example of such a reaction, where there is almost no neutron generation, is the fusion reaction between protons (p) and boron (^{11}B) nuclei. Here, the energy is released as the kinetic energy of alpha particles rather than neutrons.

Such a reaction can be carried out in the Plasma-Focus system using the injection of boron directly into the hot hydrogen plasma produced in PF

The work will consist in the planning and execution of a boron cloud compression experiment ablated from the PF-24 system anode using a laser beam. And further development of a method for measuring the amount of proton boron products that will be generated during the experiment on the PF-24 system.

6. SUMMARY

Plasma-Focus (PF) devices have been and are being extensively investigated by many teams throughout the world, using both small and large installations. Although PF devices have ceased to be considered as fusion reactors and have disappeared from large plasma research laboratories, that physical phenomena occurring in these devices are widely studied in small laboratories and academic centers due to low cost of plasma-focus experiments. This is certainly one of the good investigated and diagnosed plasma (more than a few thousand references could be given), but many essential facts are still unclear, yet. It providing strong

motivation for future studies in this field. As in other plasma research, the complexity of the phenomena has proved to be greater than expected. So, some of existing, important issues related to phenomena in PF still need clarification, but there are also those whose description and explanation are accepted in the scientific community. For example, the travels up of current sheath via the Lorentz force along the electrodes has been well measured by the current probes and they are consistent with the calculation by snow-plow and/or MHD model . Then, once the sheath reaches the end of the anode, it is imploded radially towards the axis of the device to formed a pinch plasma. The imploding velocity the plasma sheath is measured by the streak camera and it is consistent with the modelling, also.

The formation and breaks of the pinch plasma due to instability is accompanied by the emission of neutrons and X-rays . For many years, there was a large debate about whether the neutrons were emitted by thermal plasma. Since this was, indeed, a most important point, there was a very large effort to make measurements under various types of experimental procedures. At present, we are agreed, that this issue is settled, in the sense that, whatever device is used, in regimes when large neutron yields are created, the emission is due to the bombardment of accelerated deuterons onto the deuterium ions from the plasma, or even the cold deuterium that fills the chamber. Similarly, the high X-ray emission, occurring together with neutron emission, are primarily the result of braking the accelerated electrons on the anode, as in X-ray tubes. However, let us looked on the main issues requiring further investigations.

One question that can be asked is the influence of the structure of a plasma sheath on the emission of particles (ions, electrons and neutrons). For example, differences in the results obtained by two devices used to study neutron emission characteristics are not necessarily due to different physical behaviors (e.g. types of instability), but rather due to the difference in the formation of the plasma sheath as the results of different initial conditions. Systematic study of the relationship between the initial sheath structure, its evolution along the PF electrodes and its influence on the beam generation is one example of a study that has not yet been done, due to the broad scope of this investigations.

The second important question is whether one cause or a single physical phenomenon may be responsible for the different properties of the beams emitted by the plasma focus. This would be confirmed by the fact that many PF plasmas have similar general behavior, which is a qualitative indicator that this can be indeed the case. However, despite the attractiveness of this view, there is certainly not enough experimental evidence to support it, and this is one of the interesting research topics.

The future research program dedicated to PF-24 can be formulated based on the following three general research directions:

1. One of the main issues to examine is the detailed physics of the electric breakdown of a working gas, the formation and structure of the plasma sheath and its propagation along PF electrodes. The aim is to determine the structure of the plasma sheath, its curvature and how it leads to the generation of fast particles. Such knowledge should eventually make it possible to understand the currently puzzling difference in the behavior of the nuclear phase in the PF plasma. Furthermore, it seems that understanding this issue would enable the construction of a system in which the emission of electron, ion beams as well as and neutrons would be repeatable from

discharge to discharge. This is important if we want to propose this system for commercial applications

2. The second issue should be explanation physical phenomena connected with a generation of electron and ion beams during the nuclear phase of the PF discharge and linked them with the spatial and time distributions of fast particles emitted from the pinch plasma. For this purpose, there should be performed simultaneous measurements of the electron and ion parameters.
3. Third topic of research is decoupling of the early phases of PF discharge from final stage in which in which the beams are generated. . A commonly used method of modifying a composition of plasma and its density in a compressed plasma column is the gas injection method through a high-speed electromagnetic valve located in the PF anode or the installation of a coaxial liner on the anode front. However, there is a limitation on the liner density, which far exceeds that of the current sheath even when the PF discharge is initiated in a heavy gas. So, instead of these methods, we propose to use laser ablation from the samples made with different isotopes, which can placed in the selected area of the PF anode
4. Other promising topic related to adding the high Z elements by laser ablation, to the pinch plasma is investigation of the radiative plasma compression and its influence on generation of a fast particle in the PF.

All research topics presented can be implemented on the Plasma Focus device at IFJ PAN. Although currently available diagnostic equipment is limited to the apparatus discussed earlier, further extension of the experimental facilities is possible for the existing PF construction.

REFERENCES:

Akel M., Ł. Marciniak, S. Ismael, D. Gannom, A. Kulińska, S. Lee, M. Scholz, H.-J. Kunze, S. H. Saw (2019), *Investigation of the Measured and Computed Neutron Yield From the PF-24 Device Operated With D_2-x%Ar Admixture*, IEEE Transactions on Plasma Science **47** 4301,

Anisimov S.I., D. Bäurele, B. S. Luk'yanchuk (1993), *Gas dynamics and film profiles in pulsed-laser deposition of materials*, Phys. Rev. B, 48, 12076

Basque G., A. Jolas, J.P. Watteau (1968), *Comparision of a two-dimensional snowplough model with experiment* Phys. Fluids. **11** 1384-1386

Bennett N., M. Blasco, K. Breeding et al. (2017), *Development of the dense plasma focus for short-pulse applications*, Physics of Plasmas **24**, 012702

Bernard A., H. Bruzzone, P. Choi, V. Gribkov, J. Herrera, K. Hirano, A. Krejci, S. Lee, C. Luo, F. Mezzetti, M. Sadowski, H. Schmidt, K. Ware, C.S. Wong, V. Zoita (1998), *Scientific status of plasma focus research* J. Moscow Phys. Soc. **8** 93-170

Bielecki J., K. Drozdowicz, D. Dworak, A. Igielski, W. Janik, A. Kulińska, Ł. Marciniak, M. Scholz, M. Turzański, U. Wiącek, U. Woźnicka and A. Wójcik-Gargula (2018), *Experimental and MONTE CARLO investigations of BCF-12 small-area plastic scintillation detectors for neutron pinhole camera*, Radiation Protection Dosimetry **180** (2018) 427-431

Bielecki J., A. Wójcik-Gargula, U. Wiącek, M. Scholz, A. Igielski, K. Drozdowicz, U. Woźnicka (2015), *A neutron pinhole camera for PF-24 source: Conceptual design and optimization,* Eur. Phys. J. Plus, **130** 145

Bieńkowska B., R. Prokopowicz, M. Scholz, J. Kaczmarczyk, A. Igielski, L. Karpiński, M. Paduch, and K. Pytel (2014), *Neutron counter based on beryllium activation*, AIP Conference Proceedings, **1612** 105

Braginski S.I., A.B. Migdal (1958), Fizika Plazmy i Probliema Upravlaiemych Tiermojadiernych Reakcji **2** 20-25

Decker G., R. Wienecke (1976)*, Plasma focus devices* Physica B+C **82** 155-164

Erhardt J., P. Kirchesch, K. Hubner, and J.P. Rager (1982), *Light-Scattering in the Frascati Plasma Focus*, Physics Lett. **89A** 285.

Filippov N.V. (1983), *Plasma-Focus Experiments at the Kurchatov Institute Moscow (Review)* Fizika Plasmy **9** 25-44

Filippov, N.V., Filippova, T.I., Vinogradov, V.P. (1962), *Dense, high-temperature plasma in a noncylindrical 2-pinch compression*. Nuclear Fusion Supplement. Vol. Pt2, p. 577

Gourlan C., H. Kroegler, Ch. Maisonnier, J.P. Rager, B.V. Robouch and A. Gentilini (1979), *Recent Progress in 1-MJ Plasma Focus Dynamics and Scaling for Neutron Production*, Proc. 7th Int. Conf. on Plasma Physics and Controlled Nuclear Fusion Research, Innsbruck, Austria, 23-30 August 1978. Nuclear Fusion suppl., Vol. II, IAEA-CN-37, p. 123-134

Gribkov V.A., N.V. Filippov (1979), Preprint FI AN Sov. Union, **94**

Haines M.G. (2011), *A review of the dense Z-pinch*, Plasma Physics and Controlled Fusion, **53** 093001, pp. 1–168

Herold H., A. Jerzykiewicz, M. Sadowski and H. Schmidt (1989), *Comparative analysis of large plasma focus experiments performed at IPF, Stuttgart, and IPJ, Świerk*, Nuclear Fusion **29** 1255-1266

Król K. (2015), *Wyznaczanie parametrów generatora prądowego układu Plasma Focus 24*, Raport wewnętrzny, 2015

Lee S. (2014), *Plasma Focus Radiative Model: Review of the Lee Model Code* J. Fusion Energ. **33** 4

Lee S. (2017), http://www.plasmafocus.net (2017). Accessed 26 Apr 2018

Lee S., S. H. Saw (2017), *The Plasma Focus – Numerical Experiments, Insights and Applications*, Plasma Science and Technology for Emerging Economies, pages 113–232, DOI: 10.1007/978-981-10-4217-1_3, online ISBN: 978-981-10-4217-1, print ISBN: 978-981-10-4216-4

Lee S., S.H. Saw (2008a), *Neutron Scaling Laws from Numerical Experiments*, J. Fusion Energ. **27** 4

Lee S., S.H. Saw (2008b), Pinch current limitation effect in plasma focus ,A.I.P. Appl, Phys. Lett. **92** 021503

Lehner G. (1970), *Reaction Rates and Energy Spectra for Nuclear Reactions in High Energy Plasmas*, Z. Physik **232** 174

Liberman M.A., J.S. De Groot, A. Toor, R.B. Spielman (1999), *Physics of High-Density Z-Pinch Plasmas*, 1999, DOI:10.1007/978-1-4612-1424-3, online ISBN: 978-1-4612-1424-3, print ISBN: 978-1-4612-7138-3

Marciniak Ł. (2020), *Investigation of plasma compression in the PF-24 device with the use of different Z working gases*, PhD Thesis, IFJ PAN, Kraków, Poland

Marciniak Ł., M. Akel, A. Kulińska, M. Scholz, S. Lee, H.-J. Kunze, S. H. Saw (2018), *Measurements and Simulations of Neutron Emission Versus Deuterium Filling Pressure in Plasma Focus Device PF-24*, J. Fusion Energ. **37** 124

Marciniak Ł., M. Akel, A. Kulińska, S. Lee, H.-J. Kunze, M. Scholz, S. H. Saw (2020), *Results of plasma radiative compression investigation in the PF-24 device operated with D_2, Ar and (100%-x)D_2-x%Ar mixtures obtained using the 5-phase Lee model code,* Plasma Physics and Controlled Fusion, submitted, March 2020: PPCF-102867

Marciniak Ł., A. Wójcik-Gargula, A. Kulińska, J. Bielecki, U. Wiącek (2016), *Diagnostic systems for the nuclear fusion and plasma research in the PF-24 plasma focus laboratory at the IFJ PAN*, Nukleonika **61** 413

Mather J.W. (1965), *Formation of a High-Density Deuterium Plasma Focus* Phys. Fluids **8** 366-377

Mather J.W. (1971), *Dense Plasma Focus*, Methods of Experimental Physics **9** 187

Michel L., K.H. Schonbach, H. Fisher (1974), *Neutron emission from a small 1 kJ Plasma Focus* Appl. Phys. Letters **24** 57-59

Moreau D.C. (1977), *Potentiality of the proton-boron fuel for controlled thermonuclear fusion*, Nucl. Fusion **17** 1

Sadowski M., M. Scholz (2008), *The main issues of research on dense magnetized plasmas in PF discharge* Plasma Sources Sci. Technol. **17** 024001

Sadowski M.J., M. Scholz (2012), *Important issues in high-current plasma experiments of the Z-pinch type*, Nukleonika, **57** 11–24

Scholz M. (2008), *Megajoule Plasma-Focus Facility as a Generator of Intense Fast Neutron Pulses. Dense Z-pinches,* Alexandria, VA, USA, August 17-21, 2008.

Scholz M. (2016), *Plasma-Focus and controlled nuclear fusion*, IFJ PAN, Kraków, 2016, ISBN 978-83-63542-56-6

Scholz M., J. Bielecki, A. Wójcik-Gargula, U. Wiącek, K. Drozdowicz, A. Igielski, A. Kulińska, G. Tracz, U. Woźnicka (2014), *Assumptions for the design of a neutron pinhole camera dedicated to the PF-24 device*, IFJ Report, 2073/AP

Scholz M, B. Bieńkowska, L.M. Ivanova-Stanik, L. Karpiński, M. Paduch, K. Tomaszewski, E. Zielinska, J. Kravarik, P. Kubes, A. Banaszak, L. Jakubowski, M. Sadowski, A. Szydłowski, H. Schmidt, S. Vitulli (2004), *Correlation between pinch dynamics, neutron, and X-ray emission from megajule plasma focus device* Vacuum **76** 361-364

Scholz M., K. Król, A. Kulińska, L. Karpiński, A. Wójcik-Gargula, M. Fitta (2019), *On the Possibility of Initiating the Proton-Boron Nuclear Fusion Reaction in the Plasma-Focus Device*, J. Fusion Energ. **38** 522

Scholz M., W. Stępniewski, B. Bieńkowska, L. Ivanova-Stanik, R. Miklaszewski, M. Paduch, M. Sadowski, and K. Tomaszewski (2005), *Progress in Numerical Modelling of Plasma-Focus Discharge* PLASMA 2005: Int. Conf. on Research and Applications of Plasmas, 6-9 September 2005 Opole-Turawa, Poland. AIP Conf. Proc. **812** 57-63

Shearer J.W. (1976), *Contraction of Z pinches actuated by radiation losses*, Physics of Fluids, **19**, 1426–1428

Soto L., P. Silva, J. Moreno, M. Zambra, W. Kies, R. E. Mayer, L. Altamirano, C. Pavez, L. Huerta (2008), *Demonstration of neutron production in a table top pinch plasma focus device operated at only tens of joules*. J. Phys. D: Appl. Phys. **41** 205215

PUBLISHING RESEARCH CONDUCTED IN PF-24

1. A.Kurowski, M. Scholz, A. Igielski, A. Kulińska
   Laboratorium aparaturowych źródeł neutronów im. prof. Jana A. Czubka w IFJ PAN
   Badania i rozwój technologii dla kontrolowanej fuzji termojądrowej
   Red. U. Woźnicka, (IFJ PAN, Kraków); ISBN 978-83-63542-28-3 (2014) 50-61.
2. M. Scholz, J. Bielecki, A. Wójcik-Gargula, U. Wiącek, K. Drozdowicz,A. Igielski, A. Kulińska, G. Tracz,
   U. Woźnicka
   Assumptions for the design of a neutron pinhole camera dedicated to the PF-24 device
   IFJ Report, 2073/AP (2014)
3. Bieńkowska, R. Prokopowicz, M. Scholz, J. Kaczmarczyk, A. Igielski, L. Karpiński, M. Paduch, K. Pytel
   Neutron counter based on beryllium activation
   AIP Conf. Proc., 1612 (2014) 105
4. J. Bielecki, A. Wójcik-Gargula, U. Wiącek, M. Scholz, A. Igielski, K. Drozdowicz, U. Woźnicka
   A neutron pinhole camera for PF-24 source: Conceptual design and optimization
   Eur. Phys. J. Plus, 130 (2015) 145, doi: 10.1140/epjp/i2015-15145-x
5. G. Tracz, U. Wiącek and B.Bieńkowska
   Monte Carlo simulations of neutron and photon radiation fields at the PF-24 plasma focus device at IFJ PAN in Krakow
   IFJ Report, 2091/AP (2016)

6. Ł. Marciniak, A. Wójcik-Gargula, A. Kulińska, J. Bielecki, U. Wiącek
Diagnostic systems for the nuclear fusion and plasma research in the PF-24 plasma focus laboratory at the IFJ PAN
Nukleonika, 61 (2016) 413, doi: 10.1515/nuka-2016-0068,

7. J. Bielecki, A. Wójcik-Gargula, M. Scholz
Conceptual design of the tomographic system for simultaneous studying of soft and hard X-ray emission from dense magnetized plasma
Fusion Eng. Des. 11 (2016) 646, doi:/10.1016/j.fusengdes.2016.04.030

8. J. Bielecki, K. Drozdowicz, D. Dworak, A. Igielski, W. Janik, A. Kulińska, Ł. Marciniak, M. Scholz, M. Turzański, U. Wiącek, U. Woźnicka and A. Wójcik-Gargula
Experimental and MONTE CARLO investigations of BCF-12 small-area plastic scintillation detectors for neutron pinhole camera
Radiation Protection Dosimetry 180 (2018) 427, doi:10.1093/rpd/ncx277.

9. Ł. Marciniak, M. Akel, A. Kulińska, M. Scholz, S. Lee, H.-J. Kunze, S. H. Saw
Measurements and Simulations of Neutron Emission Versus Deuterium Filling Pressure in Plasma Focus Device PF-24
Journal of Fusion Energy 37 (2018) 124, doi:10.1007/s10894-018-0157-2

10. M. Akel, Ł. Marciniak, S. Ismael, D. Gannom, A. Kulińska, S. Lee, M. Scholz, H.-J. Kunze, S. H. Saw,
Investigation of the Measured and Computed Neutron Yield From the PF-24 Device Operated With D_2-x%Ar Admixture
IEEE Transactions on Plasma Science 47 (2019) 4301, DOI: 10.1109/TPS.2019.2932182

11. M. Scholz, K. Król, A. Kulińska, L. Karpiński, A. Wójcik-Gargula, M. Fitta
On the Possibility of Initiating the Proton-Boron Nuclear Fusion Reaction in the Plasma-Focus Device
Journal of Fusion Energy 38 (2019) 522, DOI: 10.1007/s10894-019-00225-5

12. Ł. Marciniak
Investigation of plasma compression in the PF-24 device with the use of different Z working gases
PhD Thesis, IFJ PAN, Kraków, Poland, 2020

13. Ł. Marciniak, M. Akel, A. Kulińska, S. Lee, H.-J. Kunze, M. Scholz, S. H. Saw
Results of plasma radiative compression investigation in the PF-24 device operated with D_2, Ar and
(100%-x)D_2-x%Ar mixtures obtained using the 5-phase Lee model code
Plasma Physics and Controlled Fusion, submitted, March 2020: PPCF-102867